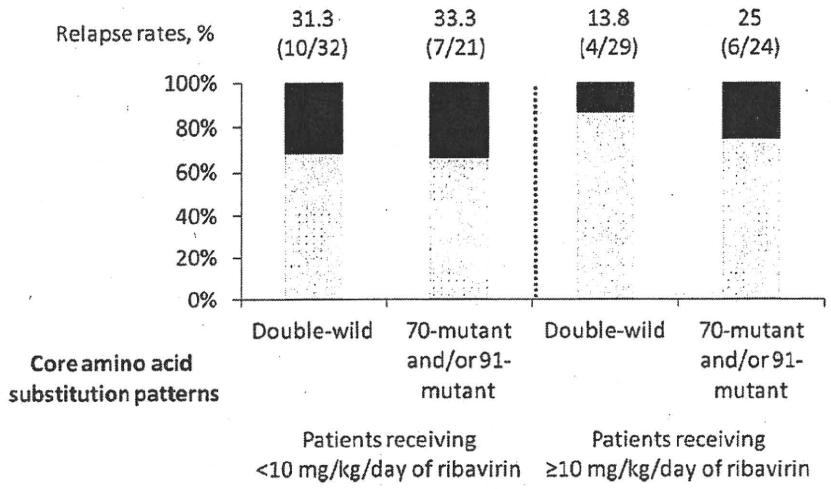

Fig. 3. Relapse rates according to core amino acid substitution patterns in patients receiving <10 mg/kg/day and receiving ≥10 mg/kg/day of ribavirin. Relapse rates are shown as percentages and the number of patients with relapse in relation to the total number of patients examined is shown at the top of each column. Gray bar, sustained virological response; black bar, relapse.

terns were similarly found in age, platelet count, and γ-GTP level. Accordingly, this study cohort had no specific bias and seems to reflect the natural background of the patients according to the HCV variance. In this study, the impact of HCV core aa substitutions on the virological response were evaluated by multivariate analysis, in order to resolve the bias of patient background factors among the groups classified according to the core aa substitution patterns. Recently, Abe et al. [2010] reported that the human genotype of the rs8099917 SNP at the IL28B locus was associated with lower γ-GTP level and viral wild type of core aa 70 and 91. Possibly these differences of IL28B genotype may influence the difference of patient background factors. Further studies are needed to clarify the relationship between human genetic variation and HCV core amino acid substitutions.

The HCV core protein has been reported to have an effect on a variety of cellular functions [Lai and Ware, 2000; Joo et al., 2005; Ariumi et al., 2007; Waris et al., 2007; Osna et al., 2008]. Currently, aa substitutions in the HCV core region has been thought to be related with outcome of antiviral therapy [Akuta et al., 2005; Donlin et al., 2007] and also the development of hepatocellular carcinoma [Akuta et al., 2007a; Hu et al., 2009]. Importance of core aa substitutions, especially at aa 70 and 91, comes to be recognized, and the new method to detect these substitutions easily has been proposed [Nakamoto et al., 2009]. As for the mechanism of antiviral activity on core aa substitutions, Ikeda et al. [2010] showed that core aa substitutions were not associated with intracellular antiviral response to IFN-alpha by in vitro analysis. The mechanism of antiviral activity and hepatocarcinogenesis on core aa substitutions has not been elucidated enough, so far. Further in vitro studies will be needed to clarify this.

Previous studies showed that patients with substitution of core aa 70 often had slow or no decrease in HCV RNA levels during the early phase of IFN-alpha treatment [Akuta et al., 2005, 2007b,c; Donlin et al., 2007]. Consistent with these reports, multivariate analysis in this study revealed that substitution of core aa 70 could be independently associated with insufficient viral decline during the first 12 weeks after the treatment (decline of <1 log from baseline at week 4, <2 log at week 12). This suggests that patients with substitution of core aa 70 are likely to fail to have a sustained virological response. On the other hand, dose exposure of Peg-IFN during the first 4 weeks of treatment was also independently linked to a minimal decline in HCV RNA (<1 log) at week 4 in this study. This suggests that maintaining the dose of Peg-IFN as high as possible until the disappearance of HCV RNA can help avoid treatment failure [McHutchison et al., 2002; Oze et al., 2009], especially in patients with substitution of core aa 70. On the other hand, substitution of core aa 91 was independently associated with detectable HCV RNA at week 24. This suggests that patients with substitution of core aa 91 are likely to achieve non-sustained virological response even if they had a ≥2 log decline in the HCV RNA level at week 12. The reason for the difference of the impact on virological response is not yet clear.

Multivariate logistic regression analysis also showed that the dose exposure of ribavirin during the full treatment period and having late virological response were independently associated with relapse. As for ribavirin exposure, it has been previously demonstrated that the relapse rate among patients responding to the treatment showed a decline in relation to the increase in the dose of ribavirin [Hiramatsu et al., 2009]. In this study, relapse rates were also decreased from 36% to 13.3% with increasing dose exposure of ribavirin among patients with end-of-treatment response. These results

confirm that maintaining a sufficient dose of ribavirin during the full treatment period could reduce the possibility of relapse, and that an extended duration of therapy for patients with late virological response could increase the chance of achieving sustained virological response, regardless of core aa substitution patterns [Berg et al., 2006; Pearlman et al., 2007; Ferenci et al., 2010].

In this study, the COBAS Amplicor HCV Test v2.0, with a lower limit of detection of 50 IU/ml, was used to assess the serum HCV RNA. Recently, real-time PCR-based HCV RNA assays with a higher sensitivity, COBAS TaqMan HCV assay (Chugai-Roche Diagnostics), with a lower limit of detection of 15 IU/ml, have been introduced. Sarrazin et al. [2010] compared virological response rates that were originally tested by COBAS Amplicor assay with those retested by COBAS TaqMan assay, using the same cohort. Among genotype 1 patients, complete early virological response and sustained virological response rates were similar when virological responses were defined as <50 IU/ml by Amplicor assay (77% and 87%) and <15 IU/ml by TaqMan assay (76% and 88%). Therefore, measuring HCV RNA by the Amplicor assay in this study would have little affects on the results.

In conclusion, the results have demonstrated that substitution of core aa 70 could be independently associated with an insufficient decline in HCV RNA level during first 12 weeks, and substitution of core aa 91 was independently associated with detectable HCV RNA at week 24, all of which were considered to be important negative predictors of attaining sustained virological response in patients with HCV genotype 1 treated with Peg-IFN plus ribavirin. On the other hand, only dose exposure of ribavirin and no complete early virological response was independent predictors of virological relapse among patients with end-of-treatment response, not substitution of core aa 70 or 91. The aa substitution patterns of the HCV core protein can be an important pretreatment predictor for non-response in patients with HCV genotype 1 treated with Peg-IFN plus ribavirin, but not for relapse after the completion of therapy.

REFERENCES

Abe H, Ochi H, Maekawa T, Hayes CN, Tsuge M, Miki D, Mitsui F, Hiraga N, Imamura M, Takahashi S, Ohishi W, Arihiro K, Kubo M, Nakamura Y, Chayama K. 2010. Common variation of IL28 affects gamma-GTP levels and inflammation of the liver in chronically infected hepatitis C virus patients. J Hepatol 53:439–443.

Akuta N, Suzuki F, Sezaki H, Suzuki Y, Hosaka T, Someya T, Kobayashi M, Saitoh S, Watahiki S, Sato J, Matsuda M, Arase Y, Ikeda K, Kumada H. 2005. Association of amino acid substitution pattern in core protein of hepatitis C virus genotype 1b high viral load and non-virological response to interferon-ribavirin combination therapy. Intervirology 48:372–380.

Akuta N, Suzuki F, Kawamura Y, Yatsuji H, Sezaki H, Suzuki Y, Hosaka T, Kobayashi M, Arase Y, Ikeda K, Kumada H. 2007a. Amino acid substitutions in the hepatitis C virus core region are the important predictor of hepatocarcinogenesis. Hepatology 46:1357–1364.

Akuta N, Suzuki F, Kawamura Y, Yatsuji H, Sezaki H, Suzuki Y, Hosaka T, Kobayashi M, Arase Y, Ikeda K, Kumada H. 2007b. Predictive factors of early and sustained responses to peginterferon plus ribavirin combination therapy in Japanese patients infected with hepatitis C virus genotype 1b: Amino acid substitutions in the core region and low-density lipoprotein cholesterol levels. J Hepatol 46:403–410.

Akuta N, Suzuki F, Kawamura Y, Yatsuji H, Sezaki H, Suzuki Y, Hosaka T, Kobayashi M, Arase Y, Ikeda K, Kumada H. 2007c. Predictors of viral kinetics to peginterferon plus ribavirin combination therapy in Japanese patients infected with hepatitis C virus genotype 1b. J Med Virol 79:1686–1695.

Anonymous. 2002. National Institutes of Health Consensus Development Conference Statement: Management of hepatitis C: 2002—June 10–12, 2002. Hepatology 36:S3–S20.

Ariumi Y, Kuroki M, Abe K, Dansako H, Ikeda M, Wakita T, Kato N. 2007. DDX3 DEAD-box RNA helicase is required for hepatitis C virus RNA replication. J Virol 81:13922–13926.

Bedossa P, Poynard T. 1996. An algorithm for the grading of activity in chronic hepatitis C. The METAVIR Cooperative Study Group. Hepatology 24:289–293.

Berg T, von Wagner M, Nasser S, Sarrazin C, Heintges T, Gerlach T, Buggisch P, Goeser T, Rasenack J, Pape GR, Schmidt WE, Kallinowski B, Klinker H, Spengler U, Martus P, Alshuth U, Zeuzem S. 2006. Extended treatment duration for hepatitis C virus type 1: Comparing 48 versus 72 weeks of peginterferon-alfa-2a plus ribavirin. Gastroenterology 130:1086–1097.

Blindenbacher A, Duong FH, Hunziker L, Stutvoet ST, Wang X, Terracciano L, Moradpour D, Blum HE, Alonzi T, Tripodi M, La Monica N, Heim MH. 2003. Expression of hepatitis c virus proteins inhibits interferon alpha signaling in the liver of transgenic mice. Gastroenterology 124:1465–1475.

Bode JG, Ludwig S, Ehrhardt C, Albrecht U, Erhardt A, Schaper F, Heinrich PC, Haussinger D. 2003. IFN-alpha antagonistic activity of HCV core protein involves induction of suppressor of cytokine signaling-3. FASEB J 17:488–490.

Davis GL, Wong JB, McHutchison JG, Manns MP, Harvey J, Albrecht J. 2003. Early virologic response to treatment with peginterferon alfa-2b plus ribavirin in patients with chronic hepatitis C. Hepatology 38:645–652.

de Lucas S, Bartolome J, Carreno V. 2005. Hepatitis C virus core protein down-regulates transcription of interferon-induced antiviral genes. J Infect Dis 191:93–99.

Dienstag JL, McHutchison JG. 2006. American Gastroenterological Association medical position statement on the management of hepatitis C. Gastroenterology 130:225–230.

Donlin MJ, Cannon NA, Yao E, Li J, Wahed A, Taylor MW, Belle SH, Di Bisceglie AM, Aurora R, Tavis JE. 2007. Pretreatment sequence diversity differences in the full-length hepatitis C virus open reading frame correlate with early response to therapy. J Virol 81: 8211–8224.

Ferenci P, Fried MW, Shiffman ML, Smith CI, Marinos G, Goncales FL, Jr., Haussinger D, Diago M, Carosi G, Dhumeaux D, Craxi A, Chaneac M, Reddy KR. 2005. Predicting sustained virological responses in chronic hepatitis C patients treated with peginterferon alfa-2a (40 KD)/ribavirin. J Hepatol 43:425–433.

Ferenci P, Laferl H, Scherzer TM, Maieron A, Hofer H, Stauber R, Gschwantler M, Brunner H, Wenisch C, Bischof M, Strasser M, Datz C, Vogel W, Loschenberger K, Steindl-Munda P. 2010. Peginterferon alfa-2a/ribavirin for 48 or 72 weeks in hepatitis C genotypes 1 and 4 patients with slow virologic response. Gastroenterology 138:503–512 e501.

Fried MW, Shiffman ML, Reddy KR, Smith C, Marinos G, Goncales FL, Jr., Haussinger D, Diago M, Carosi G, Dhumeaux D, Craxi A, Lin A, Hoffman J, Yu J. 2002. Peginterferon alfa-2a plus ribavirin for chronic hepatitis C virus infection. N Engl J Med 347:975–982.

Ge D, Fellay J, Thompson AJ, Simon JS, Shianna KV, Urban TJ, Heinzen EL, Qiu P, Bertelsen AH, Muir AJ, Sulkowski M, McHutchison JG, Goldstein DB. 2009. Genetic variation in IL28B predicts hepatitis C treatment-induced viral clearance. Nature 461: 399–401.

Hadziyannis SJ, Sette H, Jr., Morgan TR, Balan V, Diago M, Marcellin P, Ramadori G, Bodenheimer H, Jr., Bernstein D, Rizzetto M, Zeuzem S, Pockros PJ, Lin A, Ackrill AM. 2004. Peginterferon-alpha2a and ribavirin combination therapy in chronic hepatitis C: A randomized study of treatment duration and ribavirin dose. Ann Intern Med 140:346–355.

Hiramatsu N, Oze T, Yakushijin T, Inoue Y, Igura T, Mochizuki K, Imanaka K, Kaneko A, Oshita M, Hagiwara H, Mita E, Nagase T,

Ito T, Inui Y, Hijioka T, Katayama K, Tamura S, Yoshihara H, Imai Y, Kato M, Yoshida Y, Tatsumi T, Ohkawa K, Kiso S, Kanto T, Kasahara A, Takehara T, Hayashi N. 2009. Ribavirin dose reduction raises relapse rate dose-dependently in genotype 1 patients with hepatitis C responding to pegylated interferon alpha-2b plus ribavirin. J Viral Hepat 16:586–594.

Hu Z, Muroyama R, Kowatari N, Chang J, Omata M, Kato N. 2009. Characteristic mutations in hepatitis C virus core gene related to the occurrence of hepatocellular carcinoma. Cancer Sci 100:2465–2468.

Ikeda F, Dansako H, Nishimura G, Mori K, Kawai Y, Ariumi Y, Miyake Y, Takaki A, Nouso K, Iwasaki Y, Ikeda M, Kato N, Yamamoto K. 2010. Amino acid substitutions of hepatitis C virus core protein are not associated with intracellular antiviral response to interferon-alpha in vitro. Liver Int 30:1324–1331.

Joo M, Hahn YS, Kwon M, Sadikot RT, Blackwell TS, Christman JW. 2005. Hepatitis C virus core protein suppresses NF-kappaB activation and cyclooxygenase-2 expression by direct interaction with IkappaB kinase beta. J Virol 79:7648–7657.

Kato N, Hijikata M, Ootsuyama Y, Nakagawa M, Ohkoshi S, Sugimura T, Shimotohno K. 1990. Molecular cloning of the human hepatitis C virus genome from Japanese patients with non-A, non-B hepatitis. Proc Natl Acad Sci USA 87:9524–9528.

Kobayashi M, Akuta N, Suzuki F, Hosaka T, Sezaki H, Suzuki Y, Arase Y, Ikeda K, Watahiki S, Mineta R, Iwasaki S, Miyakawa Y, Kumada H. 2010. Influence of amino-acid polymorphism in the core protein on progression of liver disease in patients infected with hepatitis C virus genotype 1b. J Med Virol 82:41–48.

Lai MM, Ware CF. 2000. Hepatitis C virus core protein: Possible roles in viral pathogenesis. Curr Top Microbiol Immunol 242:117–134.

Lin W, Kim SS, Yeung E, Kamegaya Y, Blackard JT, Kim KA, Holtzman MJ, Chung RT. 2006. Hepatitis C virus core protein blocks interferon signaling by interaction with the STAT1 SH2 domain. J Virol 80:9226–9235.

Manns MP, McHutchison JG, Gordon SC, Rustgi VK, Shiffman M, Reindollar R, Goodman ZD, Koury K, Ling M, Albrecht JK. 2001. Peginterferon alfa-2b plus ribavirin compared with interferon alfa-2b plus ribavirin for initial treatment of chronic hepatitis C: A randomised trial. Lancet 358:958–965.

McHutchison JG, Manns M, Patel K, Poynard T, Lindsay KL, Trepo C, Dienstag J, Lee WM, Mak C, Garaud JJ, Albrecht JK. 2002. Adherence to combination therapy enhances sustained response in genotype-1-infected patients with chronic hepatitis C. Gastroenterology 123:1061–1069.

McHutchison JG, Lawitz EJ, Shiffman ML, Muir AJ, Galler GW, McCone J, Nyberg LM, Lee WM, Ghalib RH, Schiff ER, Galati JS, Bacon BR, Davis MN, Mukhopadhyay P, Koury K, Noviello S, Pedicone LD, Brass CA, Albrecht JK, Sulkowski MS. 2009. Peginterferon alfa-2b or alfa-2a with ribavirin for treatment of hepatitis C infection. N Engl J Med 361:580–593.

Melen K, Fagerlund R, Nyqvist M, Keskinen P, Julkunen I. 2004. Expression of hepatitis C virus core protein inhibits interferon-induced nuclear import of STATs. J Med Virol 73:536–547.

Nakamoto S, Kanda T, Yonemitsu Y, Arai M, Fujiwara K, Fukai K, Kanai F, Imazeki F, Yokosuka O. 2009. Quantification of hepatitis C amino acid substitutions 70 and 91 in the core coding region by real-time amplification refractory mutation system reverse transcription-polymerase chain reaction. Scand J Gastroenterol 44:872–877.

Okanoue T, Itoh Y, Hashimoto H, Yasui K, Minami M, Takehara T, Tanaka E, Onji M, Toyota J, Chayama K, Yoshioka K, Izumi N, Akuta N, Kumada H. 2009. Predictive values of amino acid sequences of the core and NS5A regions in antiviral therapy for hepatitis C: A Japanese multi-center study. J Gastroenterol 44: 952–963.

Osna NA, White RL, Krutik VM, Wang T, Weinman SA, Donohue TM, Jr. 2008. Proteasome activation by hepatitis C core protein is reversed by ethanol-induced oxidative stress. Gastroenterology 134:2144–2152.

Oze T, Hiramatsu N, Yakushijin T, Kurokawa M, Igura T, Mochizuki K, Imanaka K, Yamada A, Oshita M, Hagiwara H, Mita E, Ito T, Inui Y, Hijioka T, Tamura S, Yoshihara H, Hayashi E, Inoue A, Imai Y, Kato M, Yoshida Y, Tatsumi T, Ohkawa K, Kiso S, Kanto T, Kasahara A, Takehara T, Hayashi N. 2009. Pegylated interferon alpha-2b (Peg-IFN alpha-2b) affects early virologic response dose-dependently in patients with chronic hepatitis C genotype 1 during treatment with Peg-IFN alpha-2b plus ribavirin. J Viral Hepat 16:578–585.

Pearlman BL, Ehleben C, Saifee S. 2007. Treatment extension to 72 weeks of peginterferon and ribavirin in hepatitis c genotype 1-infected slow responders. Hepatology 46:1688–1694.

Romero-Gomez M, Del Mar Viloria M, Andrade RJ, Salmeron J, Diago M, Fernandez-Rodriguez CM, Corpas R, Cruz M, Grande L, Vazquez L, Munoz-De-Rueda P, Lopez-Serrano P, Gila A, Gutierrez ML, Perez C, Ruiz-Extremera A, Suarez E, Castillo J. 2005. Insulin resistance impairs sustained response rate to peginterferon plus ribavirin in chronic hepatitis C patients. Gastroenterology 128: 636–641.

Sarrazin C, Shiffman ML, Hadziyannis SJ, Lin A, Colucci G, Ishida H, Zeuzem S. 2010. Definition of rapid virologic response with a highly sensitive real-time PCR-based HCV RNA assay in peginterferon alfa-2a plus ribavirin response-guided therapy. J Hepatol 52:832–838.

Shirakawa H, Matsumoto A, Joshita S, Komatsu M, Tanaka N, Umemura T, Ichijo T, Yoshizawa K, Kiyosawa K, Tanaka E. 2008. Pretreatment prediction of virological response to peginterferon plus ribavirin therapy in chronic hepatitis C patients using viral and host factors. Hepatology 48:1753–1760.

Strader DB, Wright T, Thomas DL, Seeff LB. 2004. Diagnosis, management, and treatment of hepatitis C. Hepatology 39:1147–1171.

Suppiah V, Moldovan M, Ahlenstiel G, Berg T, Weltman M, Abate ML, Bassendine M, Spengler U, Dore GJ, Powell E, Riordan S, Sheridan D, Smedile A, Fragomeli V, Muller T, Bahlo M, Stewart GJ, Booth DR, George J. 2009. IL28B is associated with response to chronic hepatitis C interferon-alpha and ribavirin therapy. Nat Genet 41:1100–1104.

Tanaka Y, Nishida N, Sugiyama M, Kurosaki M, Matsuura K, Sakamoto N, Nakagawa M, Korenaga M, Hino K, Hige S, Ito Y, Mita E, Tanaka E, Mochida S, Murawaki Y, Honda M, Sakai A, Hiasa Y, Nishiguchi S, Koike A, Sakaida I, Imamura M, Ito K, Yano K, Masaki N, Sugauchi F, Izumi N, Tokunaga K, Mizokami M. 2009. Genome-wide association of IL28B with response to pegylated interferon-alpha and ribavirin therapy for chronic hepatitis C. Nat Genet 41:1105–1109.

Thompson AJ, Muir AJ, Sulkowski MS, Ge D, Fellay J, Shianna KV, Urban T, Afdhal NH, Jacobson IM, Esteban R, Poordad F, Lawitz EJ, McCone J, Shiffman ML, Galler GW, Lee WM, Reindollar R, King JW, Kwo PY, Ghalib RH, Freilich B, Nyberg LM, Zeuzem S, Poynard T, Vock DM, Pieper KS, Patel K, Tillmann HL, Noviello S, Koury K, Pedicone LD, Brass CA, Albrecht JK, Goldstein DB, McHutchison JG. 2010. Interleukin-28B polymorphism improves viral kinetics and is the strongest pretreatment predictor of sustained virologic response in hepatitis C virus-1 patients. Gastroenterology 139:120–129 e118.

Waris G, Felmlee DJ, Negro F, Siddiqui A. 2007. Hepatitis C virus induces proteolytic cleavage of sterol regulatory element binding proteins and stimulates their phosphorylation via oxidative stress. J Virol 81:8122–8130.

Biochemical and Biophysical Research Communications 399 (2010) 144–149

Contents lists available at ScienceDirect

Biochemical and Biophysical Research Communications

journal homepage: www.elsevier.com/locate/ybbrc

Insulin-like growth factor binding protein-1 levels are increased in patients with IgA nephropathy

Koki Tokunaga, Hirofumi Uto *, Yoichiro Takami, Kumiko Mera, Chika Nishida, Yozo Yoshimine, Mayumi Fukumoto, Manei Oku, Atsushi Sogabe, Tsuyoshi Nosaki, Akihiro Moriuchi, Makoto Oketani, Akio Ido, Hirohito Tsubouchi

Department of Digestive and Life-Style Related Disease, Health Research Course, Human and Environmental Sciences, Kagoshima University Graduate School of Medical and Dental Sciences, 8-35-1 Sakuragaoka, Kagoshima 890-8520, Japan

ARTICLE INFO

Article history:
Received 30 June 2010
Available online 15 July 2010

Keywords:
IGFBP-1
IgA nephropathy
Serum level
Mesangial cell proliferation
IGF-1

ABSTRACT

The mechanisms underlying the pathogenesis of immunoglobulin A (IgA) nephropathy (IgAN) are not well understood. In this study, we examined gene expression profiles in kidneys obtained from mice with high serum IgA levels (HIGA mice), which exhibit features of human IgAN. Female inbred HIGA, established from the ddY line, were used in these experiments. Serum IgA levels, renal IgA deposition, mesangial proliferation, and glomerulosclerosis were increased in 32-week-old HIGA mice in comparison to ddY animals. By microarray analysis, five genes were observed to be increased by more than 2.5-fold in 32-week-old HIGA in comparison to 16-week-old HIGA; these same five genes were decreased more than 2.5-fold in 32-week-old ddY in comparison to 16-week-old ddY mice. Of these five genes, insulin-like growth factor (IGF) binding protein (IGFBP)-1 exhibited differential expression between these mouse lines, as confirmed by quantitative RT-PCR. In addition, serum IGFBP-1 levels were significantly higher in patients with IgAN than in healthy controls. In patients with IgAN, these levels correlated with measures of renal function, such as estimated glomerular filtration rate (eGFR), but not with sex, age, serum IgA, C3 levels, or IGF-1 levels. Pathologically, serum IGFBP-1 levels were significantly associated with the severity of renal injury, as assessed by mesangial cell proliferation and interstitial fibrosis. These results suggest that increased IGFBP-1 levels are associated with the severity of renal pathology in patients with IgAN.

1. Introduction

Human immunoglobulin A (IgA) nephropathy (IgAN), an immune-complex-mediated glomerulonephritis, is the most common primary chronic glomerulonephritis worldwide, with a high prevalence in Japan and Asian countries. It is characterized by deposition of predominantly IgA antibodies over the glomerular mesangium [1]. The prognosis of patients with IgAN is poor, with 10–40% of patients developing end-stage renal failure and becoming hemodialysis-dependent [2]. It has been reported that antigenic variation, genetic factors, abnormalities of the IgA1 molecule, and various inflammatory mediators play important roles in the onset and progression of IgAN [3]. The mechanisms underlying the pathogenesis and development of IgAN, however, are not well understood; thus, specific treatment on a molecular basis has not been developed.

High serum IgA (HIGA) mice, which were established from ddY mice, exhibit features seen in IgAN, such as high serum IgA levels, IgA deposition in the glomerular mesangium, and mesangial expansion [4]. HIGA mice comprise an appropriate animal model in which to conduct gene expression analysis to identify genes involved in the progression of renal diseases. Several microarray analyses using kidneys or isolated glomeruli from these mice have been reported [5–7]. In HIGA mice, however, no renal abnormalities manifest until approximately 10 weeks of age; serum IgA levels begin to increase dramatically thereafter, becoming markedly elevated by 25 weeks of age [4,6]. Histological alterations become marked by 40 weeks of age. Thus, the time points at which tissues or cells are obtained affect the results of microarray analysis. Consequently, we evaluated serum factor levels and pathological features of HIGA mice over time, focusing on the gene expression profiles in the kidney at 16 and 32 weeks.

In this study, we focused on insulin-like growth factor binding protein (IGFBP)-1, which was differentially expressed in HIGA mice kidneys in comparison with ddY mice kidneys. The insulin-like growth factors (IGFs) are growth-promoting peptides that circulate in plasma complexes with IGFBPs. Six IGFBPs have been isolated and characterized, which share ~35% sequence identity with each

* Corresponding author. Fax: +81 99 264 3504.
E-mail address: hirouto@m2.kufm.kagoshima-u.ac.jp (H. Uto).

0006-291X/$ - see front matter © 2010 Elsevier Inc. All rights reserved.
doi:10.1016/j.bbrc.2010.07.032

other, but differ in their binding specificity [8]. IGFBPs are produced by a variety of biological tissues and found in various biological fluids and may directly contribute to the development of glomerulosclerosis [9,10]. The molecular mechanism by which IGFBP-1 contributes to the pathogenesis of IgAN, however, has not been elucidated. This study provides novel insights into the role of IGFBP-1 in the pathogenesis of IgAN.

2. Materials and methods

2.1. Animals

Animal experiments utilized female inbred HIGA and ddY mice (Japan SLC, Inc., Hamamatsu, Japan). Mice were allowed free access to standard mouse chow and tap water. All animal experiments were approved by the Institutional Animal Care and Use Committee guideline of Kagoshima University.

2.2. Patients

Between 2006 and 2008, we enrolled the 58 patients diagnosed with IgA nephropathy by renal biopsy. This study was approved by the Kagoshima University Hospital and by Nanpuh Hospital. Written informed consent was obtained from all participants in the study.

2.3. Biochemical examination

Serum blood urea nitrogen (BUN) and creatinine levels in mice were measured using SPOTCHEM™ II SP-44 assay system (ARKRAY, Inc., Kyoto, Japan). Serum IgA levels were measured using an enzyme-linked immunosorbent assay (ELISA) according to the manufacturer's instructions (Bethyl, Montgomery, TX).

Serum and urine samples from patients were obtained at time of renal biopsy. Common biochemical parameters, including BUN, creatinine, fasting plasma glucose (FPG), IgA, C3, glycohemoglobin (HbA1c), peripheral blood hemoglobin, and urinary protein levels, were determined using standard laboratory methods. Estimated glomerular filtration rate (eGFR) was calculated as described by the modification of diet in renal disease (MDRD) study: $eGFR = 0.741 \times 175 \times Age^{-0.203} \times Cr^{-1.154}$ (if female: $\times 0.742$).

2.4. Histological examination

For light microscopic studies, kidneys were isolated from HIGA and ddY mice at 16 or 32 weeks of age and fixed in 10% neutralized formalin buffer solution. Samples were then embedded in paraffin and sliced at a thickness of 2–3 μm. Slices were stained with hematoxylin and eosin (HE), periodic acid-Schiff (PAS), Masson's trichrome, and periodic acid-silver methenamine (PAM).

All biopsy specimens from patients, obtained by needle biopsy, were stained with HE, PAM, PAS, and Masson-trichrome stains, and were examined by light, immunofluorescence, and electron microscopy. Mesangial cell proliferation was classified by light microscopy as follows: no hypercellularity, score 0; fewer than four mesangial cells in the peripheral mesangial area, score 1; four or five mesangial cells in a part of the mesangial area, score 2; six or seven mesangial cells in that area, score 3; more than eight mesangial cells identified in the mesangial area, score 4. The severity of mesangial cell proliferation in each case was evaluated using an index of mesangial proliferation [11]. To evaluate for adhesion, interstitial fibrosis, interstitial infiltration, tubular atrophy and arteriole hyaline change, we determined the proportion of the area in each section comprised by each abnormal structure. In addition, glomerulosclerosis was evaluated by the proportion of number of glomerulosclerosis in total glomerulus, and intimal thickness was evaluated by rate of thickness in intima/media.

For immunofluorescence microscopy, kidney tissues were embedded in Tissue-Tek OCT compound (Sakura Finetechnical Co., Ltd., Tokyo, Japan) and snap frozen in a dry ice–acetone bath. Cryostat sections, 4 μm in thickness, were stained directly with FITC-labeled goat anti-mouse IgA antiserum (Santa Cruz Biotechnology, Santa Cruz, CA), goat anti-mouse IgG or IgM antiserum (Sigma-Aldrich Inc, Saint Louis, MO), and goat anti-mouse complement C3 antiserum (Cappel Research Reagents, Costa Mesa, CA).

2.5. Gene expression profiling

Total RNA was extracted from the total renal tissue of 16- and 32-week-old mice using TRIzol Reagent (Invitrogen Life technology, Carlsbad, CA) according to the manufacturer's instructions. The pooled total RNA from five mice was subjected to expression profiling using an Affymetrix Genechip Mouse genome 430 2.0 array according to the standard protocol (Affimetrix, Santa Clara, CA). The resultant expression profiles were normalized using Gene Spring 7.3.1 software provided by Agilent Technologies (Santa Clara, CA). Genes of interest were selected by comparing the expression intensities seen in 16- and 32-week-old HIGA and ddy mice.

2.6. Quantitative RT-PCR for the detection of IGFBP-1

Template cDNA was synthesized from 1 μg total RNA using a PrimeScript™ RT reagent Kit (Takara Bio Inc., Shiga, Japan). mRNA expression levels of IGFBP-1 (Mm00833447), acyl-CoA thioesterase 2 (Mm00506625), Plasminogen activator urokinase (Mm0044 7054), acyl-CoA synthetase medium-chain family member 2 (Mm01137661) were analyzed by quantitative real-time PCR using a TaqMan Gene Expression Assay kit (Applied Biosystems, Foster, CA) on an StepOnePlus™ Real-Time PCR System. Glyceraldehyde-3-phosphate dehydrogenase (GAPDH) (Mm99999915) mRNA levels in each sample served as a reference gene to standardize the quantities of the experimental mRNAs.

2.7. ELISA for serum IGFBP-1 level in patients with IgAN or in mice

The serum levels of IGFBP-1 in patients with IgAN or in mice were determined using a RayBio Human IGF-BP-1 ELISA kit (Norcross, GA) or mouse IGFBP-1 ELISA kit (Boster Biological Technology, Wuhan, China), respectively. Twenty subjects were also examined as healthy controls.

2.8. Statistical analysis

Results are expressed as the means ± standard deviation (SD). Statistical analyses were performed using STATVIEW (version 5.0; Abacus Concepts, Berkeley, CA) or SPSS (SPSS Inc., Chicago, IL) software programs. The frequencies or means were compared between groups using Chi square test, Fisher's exact test, or Mann–Whitney *U*-test as appropriate. Pearson's correlation analyses were performed to evaluate the relationships between the various parameters. A *P*-value less than 0.05 was considered to be statistically significant.

3. Results

3.1. Biochemical and histological examination in HIGA mice

At 16 weeks of age, serum IgA levels in HIGA mice [mean ± SD; 220.1 ± 144.0 mg/dl ($n = 10$)] did not differ from those observed in

ddY mice [208.6 ± 163.7 mg/dl (n = 4)]. These levels, however, increased significantly in HIGA mice at 32 weeks of age [498.1 ± 245.5 mg/dl (n = 9)] in comparison to both in HIGA mice at 16 weeks of age and ddy mice at 32 weeks of age [203.0 ± 113.1 mg/dl (n = 5)].

Histologically, there has never been evidence of severe glomerular lesions in ddY mice at either 16 or 32 weeks of age (Fig. 1A). Although IgA deposition was seen in mesangial lesions in HIGA mice at 16 weeks of age, there were no severe glomerular lesions. By contrast, mesangial cell proliferation, matrix expansion, and glomerulosclerosis were readily apparent in HIGA mice at 32 weeks of age (Fig 1B), despite being absent from 16-week-old HIGA mice.

3.2. Expression of IGFBP-1 in mouse kidneys evaluated by cDNA microarray and RT-PCR

Gene expression profiles of whole kidneys from HIGA and ddY mice at 16 and 32 weeks of age were evaluated using an Affimetrix mouse GeneChip. Of the differentially expressed genes, 127 genes were increased 2.5-fold or greater in HIGA mice at 32 weeks of age in comparison to 16-week-old HIGA mice. Similarly, 325 genes were decreased by more than 2.5-fold in ddY mice at 32 weeks of age in comparison to levels seen at 16 weeks. Among these genes, five genes (IGFBP-1, acyl-CoA thioesterase 2 [Acot2], plasminogen activator urokinase [Plau], acyl-CoA synthetase medium-chain family member 2 [ACSM2] and transcribed locus) were paradoxically expressed between HIGA and ddY mice. In addition, expression of mRNA encoding IGFBP-1 was confirmed to be significantly higher in HIGA mice in comparison to ddY mice at 32 weeks of age, although the levels did not differ between HIGA and ddY mice at 16 weeks of age using quantitative RT-PCR (Fig. 1C). Although serum IGFBP-1 levels in mice could not be evaluated extensively because of sample limitations, serum IGFBP-1 levels tended to be higher in HIGA mice [mean ± SD; 15.0 ± 6.8 (ng/ml) (n = 3)] in comparison to those in ddy mice (9.3 ± 3.5, n = 3) at 32 weeks. In contrast, expression of mRNA encoding three other genes, including Acot2, Plau, and ACSM2, were not significantly higher in HIGA mice in comparison to ddY mice at 32 weeks of age. Unfortunately, another gene could not be examined.

3.3. Clinical significance of serum IGFBP-1 levels in patients with IgAN

Sex, age, serum BUN, serum creatinine, eGFR, and FPG were not statistically different between patients with IgAN and healthy controls (Table 1). Serum IgA and complement component C3 levels, however, were significantly higher in patients with IgAN in comparison to healthy controls. Serum IGFBP-1 levels were also higher in patients with IgAN [mean ± SD; 23.4 ± 31.1 (ng/ml)] in comparison to healthy controls (6.5 ± 8.6) (Fig. 2A). In addition, serum IGF-1 was mildly, but significantly, increased in patients with IgAN over healthy controls [685.1 ± 456.1 (pg/ml) vs. 415.0 ± 361.0].

We compared patients with high IGFBP-1 levels (high IGFBP-1 group) greater than 23 ng/ml, which is the average seen in patients with IgAN, to patients with low IGFBP-1 levels (low IGFBP-1 group) (Table 2). Serum BUN was higher, while eGFR and fasting blood sugar were lower in the high IGFBP-1 group than the low IGFBP-1 group. Positive and negative correlations were also observed between the serum IGFBP-1 levels and serum BUN (r = 0.61, p < 0.001) and eGFR (r = −0.47, p < 0.001), respectively. Although urinary protein levels did not differ between these two groups, serum IGFBP-1 levels were higher in IgAN patients with proteinuria greater than 0.5 g/day as compared to those in IgAN patients whose urinary protein levels were less than 0.5 g/day [31.2 ± 38.2 (ng/ml) vs. 13.6 ± 12.9, P = 0.02].

Histologically, we observed a positive correlation between mesangial cell proliferation and serum IGFBP-1 levels (Fig. 2B). In addition, interstitial fibrosis and infiltration, renal tubular atrophy, and arteriole hyalinosis were apparent in the high IGFBP-1 group to a much greater extent than in the low IGFBP-1 group. In contrast, the amounts of glomerulosclerosis, adhesion, and hypertrophy of the arterial intima in renal tissue did not differ between the two groups (Table 2).

4. Discussion

In this study, we observed that IGFBP-1 mRNA was upregulated in the kidneys of HIGA mice by 32 weeks of age in comparison to 16 weeks of age, but was downregulated in 32 week-old ddY mice in comparison to the same mice at 16 weeks of age. In addition, we

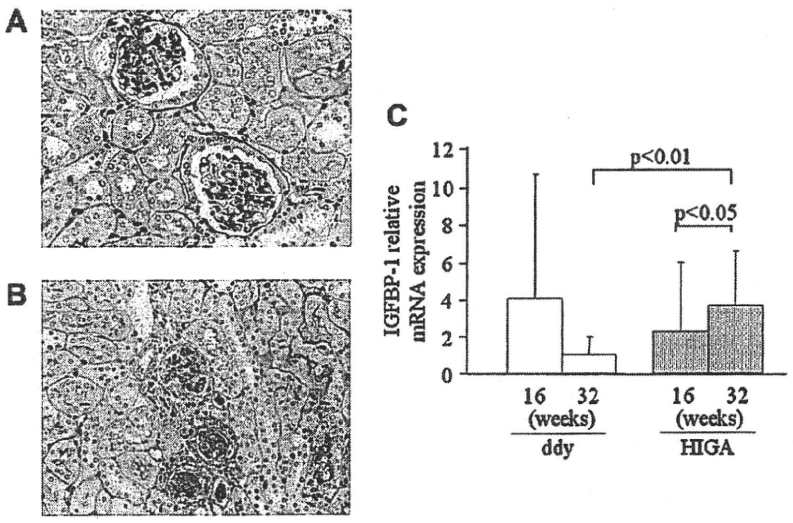

Fig. 1. Histopathological findings (A and B) or the relative expression levels of IGFBP-1 mRNA (C) in kidney tissues from HIGA or ddy mice. Although no evidence of severe glomerular lesions was observed in ddY mice at 32 weeks of age (A), mesangial cell proliferation, matrix expansion, and glomerulosclerosis were apparent in HIGA mice at 32 weeks of age (B). In addition, IGFBP-1 mRNA expression tended to decrease in ddy mice at 32 weeks of age in comparison to that seen at 16 weeks, although this difference was not significant. In contrast, IGFBP-1 mRNA expression increased significantly in HIGA mice at 32 weeks of age in comparison to 16 weeks of age. At 32 weeks of age, the expression of IGFBP-1 mRNA was significantly higher in HIGA mice in comparison to ddY mice. (A) and (B), PAS staining (×400). (C), the relative expression levels of IGFBP-1 mRNA in mouse kidneys were evaluated by quantitative real-time PCR. Determined values were normalized to GAPDH levels as a reference gene (n = 15 for each groups).

Table 1
Clinical characteristics in patients with IgA[a] nephropathy.

	IgA nephropathy (n = 58)	Healthy control (n = 20)	P-value
Female/male	33/25	11/9	0.88
Age (years)	33.26 ± 13.43	32.45 ± 6.49	0.78
Serum BUN[b] (mg/dl)	14.82 ± 4.06	13.34 ± 2.66 (n = 15)	0.25
Serum Cr[c] (mg/dl)	0.84 ± 0.41	0.76 ± 0.17 (n = 15)	0.97
eGFR[d] (ml/min/1.73m^2),	86.82 ± 29.69	83.24 ± 16.08(n = 15)	0.59
FPG[e] (mg/dl)	93.22 ± 10.15	100.10 ± 18.84 (n = 10)	0.33
Serum IgA[a] (mg/dl)	339.08 ± 120.53	255.46 ± 68.68 (n = 13)	0.02
Serum C3[f] (mg/dl)	107.15 ± 20.25	92.85 ± 11.86 (n = 13)	0.02
HbA1c (%)	5.07 ± 0.39 (I = 44)	–	–
Hemoglobin (g/dl)	13.38 ± 1.83	–	–
Proteinuria level (g/day)	0.90 ± 0.91	–	–

Data are expressed as mean ± standard deviation. p-value were obtained by a Student's t-test, or the Mann–Whitney U-test.

[a] Immunoglobulin A.

[b] Blood urea nitrogen.

[c] Creatinine.

[d] Estimated glomerular filtration rate (eGFR) are calculated in modification of diet in renal disease (MDRD) study as follows; $eGFR = 0.741 \times 175 \times Age^{-0.203} \times Cr^{-1.154}$ (female: ×0.742).

[e] Fasting plasma glucose.

[f] Complement component C3.

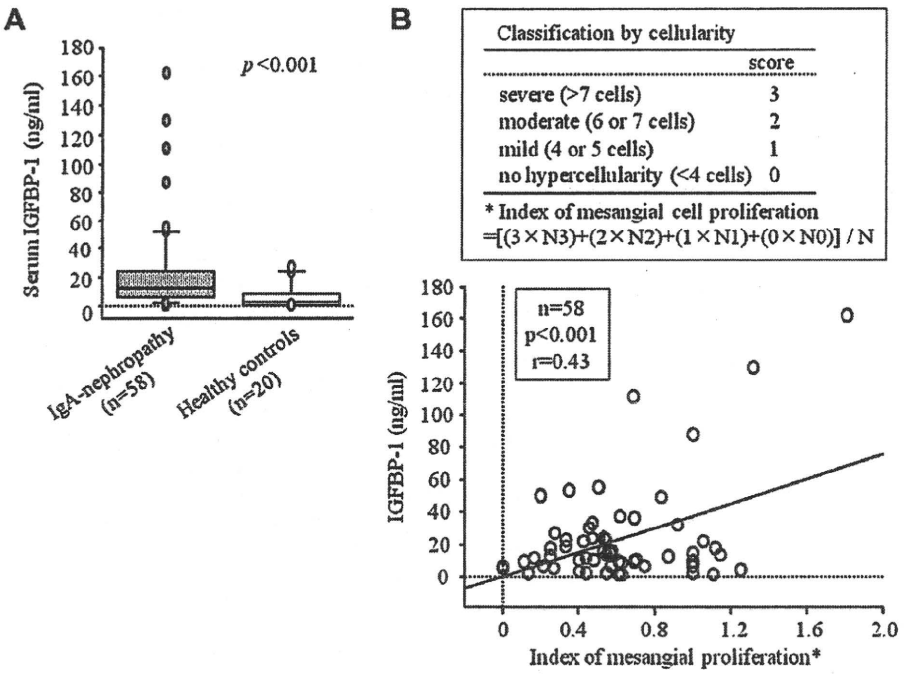

Fig. 2. Serum IGFBP-1 levels in patients with IgA nephropathy. Serum IGFBP-1 levels were significantly higher in patients with IgA nephropathy in comparison to healthy subjects (A). Boxes indicate the median ± 25th percentile. The lower and upper bars represent the 10th and 90th percentiles, respectively. In addition, the serum IGFBP-1 levels were associated with mesangial proliferation in patients with IgA nephropathy (B). The proliferation of mesangial cells in each glomerulus was scored from 0 to 3. The average for all glomeruli was calculated and registered as the index of mesangial proliferation. N0 to N3 = numbers of glomeruli showing changes of grade 0 to 3, respectively. N, N0 + N1 + N2 + N3.

observed that serum IGFBP-1 levels are higher in patients with IgAN than in healthy subjects. We also demonstrated a possible relationship between serum IGFBP-1 levels and the pathological findings of human renal tissues in IgAN.

IGFBPs play an important role in stabilizing and regulating the activity of IGF-1 and IGF-II, but also have other functions in the absence of IGFs [12]. All six IGFBPs are found circulating in a free form or as part of binary or ternary complexes with IGFs [8]. IGFBP-3, the most abundant circulating IGFBP, is associated with the progression and metastasis of certain cancers, such as ovarian cancer and colon cancer [13,14]. IGFBP-5, present at about 10% of the concentration of IGFBP-3, is also known to affect the progression of both lung and skin fibrosis [15,16]. The function of IGFBP-1, however, has not been fully elucidated. In this study, we demonstrate that serum levels of IGFBP-1 were significantly higher in patients with IgAN in comparison to healthy subjects. Previous studies have demonstrated that serum levels of IGFBP-1 are upregulated in aging or the presence of elevated plasma glucose and are downregulated by hyperinsulinemia [17,18]. Although insulin levels were not examined, age was not associated with serum IGFBP-1 levels in our study; blood glucose levels were lower in the high IGFBP-1 group in comparison with the Low IGFBP-1 group (Table 2). In addition, serum IGFBP-1 levels exhibited a negative correlation with IGF concentration in normal individuals and patients

Table 2
The characteristics with high IGFBP-1[a] group and low IGFBP-1 group.

	High (n = 16)	Low (n = 42)	P-value
IGFBP-1(ng/ml)	58.74 ± 41.64	10.00 ± 6.27	<0.001
Female/male	9/7	18/14	0.95
Age (years)	37.44 ± 13.4	31.67 ± 13.25	0.15
Serum BUN[b](mg/dl)	17.27 ± 5.63	13.88 ± 2.84	0.04
Serum Cr[c](mg/dl)	1.06 ± 0.66	0.75 ± 0.23	0.13
eGFR[d] (ml/min/1.73m^2)	72.47 ± 32.82	92.29 ± 26.84	0.02
Serum IgA[e] (mg/dl)	358.48 ± 144.88	331.69 ± 110.97	0.75
Serum C3[f](mg/dl)	98.68 ± 17.28	110.37 ± 20.38	0.05
Serum IGF-1[g] (pg/ml)	573.29 ± 365.85	717.79 ± 478.29	0.44
FPG[h](mg/dl)	88.4 ± 7.62	95.22 ± 10.48	0.02
Proteinuria level (g/day)	1.38 ± 1.37	0.72 ± 0.57(n = 41)	0.13
Histopathological findings			
Glomerulosclerosis (number/total)	0.24 ± 0.21	0.15 ± 0.03	0.12
Adhesion[i]	0.08 ± 0.11	0.08 ± 0.12	0.90
Interstitial fibrosis[i]	2.06 ± 1.12	1.31 ± 0.81	0.04
Interstitial infiltration[i]	1.81 ± 1.05	1.07 ± 0.75	0.03
Tubular atrophy[i]	1.75 ± 1.00	1.07 ± 0.75	0.02
Arteriole hyaline change (number)	7/16	5/42	0.01
Intimal thickness[j]	1.13 ± 0.96	0.64 ± 0.93	0.06

[a] Insulin-like growth factor binding protein-1.
[b] Blood urea nitrogen.
[c] Creatinine.
[d] Estimated glomerular filtration rate.
[e] Immunoglobulin A.
[f] Complement component C3.
[g] Insulin-like growth factor.
[h] Fasting plasma glucose.
[i] Proportion of injury area: >50%, 4; 25–50%, 3; 5–25%, 2;<5%, 1; no, 0.
[j] Rate of thickness in intima/media: >50%, 3; 25–50%, 2;<25%, 1; no, 0.

with diabetes mellitus [19]. Serum IGF-1 levels, however, were not different between the high and low IGFBP-1 groups. In previous studies, IGFBP-1 has been negatively correlated with creatinine clearance and positively correlated with the duration of diabetes in patients with type 2 DM [20]. Several studies in non-diabetic patients demonstrate a significant relationship between increases in IGFBP-1 levels and chronic renal failure (CRF) [21,22]. Increases in IGFBP-1 plasma levels in nephrotic patients have been reported [23]. Our study indicates that serum IGFBP-1 levels were significantly associated with elevated BUN and eGFR values in patients with IgAN, even in the absence of CRF or diabetes mellitus. Serum IGFBP-1 levels were also higher in IgAN patients with proteinuria ($\geqslant$0.5 g/day) in comparison to those with lower urinary protein levels (<0.5 g/day), even in the absence nephritis. Furthermore, elevated serum IGFBP-1 levels in patients with IgAN were associated with poor histological findings, including increased mesangial cell proliferation and interstitial fibrosis within renal tissue. We do not claim that the observations presented here are peculiar to IgAN, because of a lack of other human glomerular diseases. Regardless, these results suggest that IGFBP-1 serum levels may serve as a biomarker of decreased renal filtration, even in the absence of significant renal injury or proteinuria.

IGF-1 is a major component of the broader GH system, which also includes IGFBPs; this wide variety of growth hormones exhibits both independent and interdependent effects on cell function, growth, motility, and adhesion [24]. Perturbations in the GH system are associated with renal disease, including age-associated nephropathy, diabetic nephropathy, and end-stage renal disease [25]. Multiple studies, however, have identified conflicting effects of the GH system on renal function. Experimental data have suggested that GH may have a detrimental effect on kidney growth, scarring, and chronic kidney disease (CKD) progression [26]. IGF-1 transgenic mice display glomerular hypertrophy without glomerulosclerosis [27]. In contrast, GH therapy appears to be beneficial in reducing the morbidity and mortality of CKD [28]. Transgenic expression of IGFBP-1 selectively in mouse liver results in glomerulosclerosis without glomerular hypertrophy [10]. Our results demonstrate that serum IGFBP-1 levels were associated with more severe histological findings, including increased mesangial cell proliferation and tubular atrophy, in patients with IgAN, but not with glomerulosclerosis. Serum IGFBP-1 levels did not correlate with serum IGF-1 levels in patients with IgAN. Although this study did not analyze the entire GH system, our results suggest that IGFBP-1 affects the early stages of renal injury, which may lead to glomerulosclerosis without glomerular hypertrophy [10,29]. Thus, IGFBP-1 appears to be associated with renal injury independent of IGF-1 activity.

IGFBPs are produced by a variety of biological tissues and found in a multitude of biological fluids [30]. IGFBP-1 is produced primarily by hepatocytes [31]. Tonshoff et al. determined that hepatic production of IGFBP-1 in conjunction with decreases in renal filtration contribute to the elevated serum IGFBP-1 levels seen in pediatric patients with CRF [32]. In this study, IGFBP-1 gene expression was upregulated in the kidneys of HIGA mice at 32 weeks of age in comparison to similarly aged control ddy mice without increased production of IGFBP-1 in the liver (data not shown). As the analysis of human samples, such as hepatocytes and renal tissue, has been limited, the IgAN mouse model should help provide insight into the mechanisms by which high levels of serum IGFBP-1 function in the development of renal disease. We attempted to identify genes involved in disease progression by identifying paradoxically-expressed genes. The gene expression profiles of HIGA mice and their parental strain, ddy, may differ at a young age, such as at 16 weeks, even when the pathological findings are similar. A comparison of gene expression between HIGA and ddy mice at 32 weeks may be biased by genes that were differentially expressed at 16 weeks that may not be associated with IgAN disease progression. For this reason, we speculated that paradoxically-expressed genes may be associated with disease progression.

In this study, the paradoxical expression of IGFBP-1 in the kidney was confirmed by immunohistochemical analysis (data not shown). In ddy mice at 16 weeks of age, but not 32 weeks, IGFBP-1 immunostaining was observed in the renal tubular epithelial cells near the glomerulus. In contrast, IGFBP-1 was not detected in HIGA mice at 16 weeks old, but could be detected in renal tissues from HIGA mice at 32 weeks of age. IGFBP-1 has been reported to be expressed in several nephron segments, including the glomerulus, but not in the renal tubular epithelial cells near the glomerulus [33]. Studies examining the spatial distribution of the IGF system throughout the nephron have been performed predominantly in rats; available data from human kidneys suggest species differences [33,34]. In addition, IGFBP-1 mRNA expression in 16 week-old ddY mice was widely variable. HIGA mice were originally established from the ddY mouse line, which is quite heterogeneous. We speculate that the increases in IGFBP-1 expression in 32 week-old HIGA mice in comparison to that seen in 16 week-old HIGA mice is associated with the features of IgAN. An additional time-course examination of mRNA expression and staining in isolated early nephron segments and glomeruli from human kidney biopsy tissues will be needed.

In conclusion, serum IGFBP-1 levels are higher in patients with IgAN in comparison to healthy controls. These increased levels are associated with the severity of renal tissue injury in patients with IgAN.

References

[1] J. Berger, N. Hinglais, Intercapillary deposits of IgA–IgG, J. Urol. Nephrol. 74 (1968) 694–695.
[2] G. D'Amico, Natural history of idiopathic IgA nephropathy: role of clinical and histological prognostic factors, Am. J. Kidney Dis. 36 (2000) 227–237.

[3] B. Jonathan, F. John, IgA nephropathy, J. Am. Soc. Nephrol. 16 (2005) 2088–2097.
[4] E. Muso, H. Yoshida, E. Takeuchi, et al., Enhanced production of glomerular extracellular matrix in a new mouse stain of high serum IgA ddy mice, Kidney Int. 50 (1996) 1946–1957.
[5] S. Katsuma, S. Shiojima, A. Hirasawa, et al., Genomic analysis of a mouse model of immunoglobulin A nephropathy reveals an enhanced PDGF-EDG5 cascade, Phermacogenomics J. 1 (2001) 211–217.
[6] H. Yoshimura, M. Ito, Y. Kuwahara, et al., Downregulated expression in high IgA mice and the renal protective role of meprinβ, Life Sci. 82 (2008) 899–908.
[7] H. Yoshimura, T. Sakai, Y. Kuwahara, et al., Effects of kynurenine metabolites on mesangial cell proliferation and gene expression, Exp. Mol. Pathol. 87 (2009) 70–75.
[8] S. Rajaram, J.B. David, M. Subburaman, Insulin-like growth factor-binding proteins in serum and other biological fluids: regulation and functions, Endocr. Rev. 18 (1997) 801–831.
[9] A. Flyvbjerg, Role of growth hormone, insulin-like growth factors (IGFs) and IGF-binding proteins in the renal complications of diabetes, Kidney Int. 52 (1997) S12–S19.
[10] S. Doublier, D. Seurin, B. Fouqueray, et al., Glomerulosclerosis in mice transgenic for human insulin-like growth factor-binding protein-1, Kidney Int. 57 (2000) 2299–2307.
[11] O. Hotta, T. Furuta, S. Chiba, et al., Regression of IgA nephropathy: a repeat biopsy study, Am. J. Kidney Dis. 39 (2002) 493–502.
[12] S. Firth, R. Baxter, Cellular actions of the insulin-like growth factor binding proteins, Endoc. Rev. 23 (2002) 824–854.
[13] D. Katsaros, H. Yu, M.A. Levesque, et al., IGFBP-3 in epithelial ovarian carcinoma and its association with clinico-pathological features and patient survival, Eur. J. Cancer 37 (2001) 478–485.
[14] D. Rajaraman, W. Yang, S. Gupta, et al., The role of the insulin-like growth factor system in colorectal cancer: review of current knowledge, Int. J. Colorectal Dis. 20 (2005) 203–220.
[15] J.M. Pilewski, L. Liu, A.C. Henry, et al., Insulin-like growth factor binding protein 3 and 5 are overexpressed in idiopathic pulmonary fibrosis and contribute to extracellular matrix deposition, Am. J. Pathol. 166 (2005) 399–407.
[16] H. Yasuoka, D.M. Jukic, Z. Zhou, et al., Insulin-like growth factor binding protein 5 induces skin fibrosis: a novel murine model for dermal fibrosis, Arthritis Rheum. 54 (2006) 3001–3010.
[17] J.M.P. Holly, R.A. Biddlecombe, D.B. Dunger, et al., Circadian variation of GH-independent IGF-binding protein in diabetes mellitus and its relationship to insulin. A. New role for insulin? Clin. Endocrinol(Oxf). 29 (1988) 667–675.
[18] E.M. Rutanen, T. Karkkainen, U.H. Stenman, et al., Aging is associated with decreased suppression of insulin-like growth factor binding protein-1 by insulin, J. Clin. Endocrinol. Metab. 77 (1993) 1152–1155.
[19] I.S. Ismail, J.P. Miell, M.F. Scanion, et al., Effects of cholinergic modulation on serum insulin-like growth factor 1 and its binding proteins in normal and diabetic subjects, Clin. Endocrinol(Oxf). 42 (1995) 147–152.
[20] M. Akturk, M. Arslan, A. Altinova, et al., Association of serum levels of IGF-1 and IGFBP-1 with renal function in patients with type 2 diabetes mellitus, Growth horm. IGF. Res. 17 (2007) 186–193.
[21] J. Frystyk, P. Ivarsen, C. Skjaerbaek, et al., Serum-free insulin-like growth factor I correlates with clearance in patients with chronic renal failure, Kidney Int. 56 (1999) 2076–2084.
[22] B. Tonshoff, W.F. Blum, A.M. Wingen, et al., Serum insulin-like growth factors (IGFs) and IGF binding Proteins 1, 2, and 3 in children with chronic renal failure: relationship to height and glomerular filtration rate, J. Clin. Endocrinol. Metab. 80 (1995) 2684–2691.
[23] E.J. Richmond, A. Uzri, A.D. Rogol, The insulin-like growth factor system in kidney diseases, Nephron. 89 (2001) 5–9.
[24] Y. Zha, V.T. Le, Y. Higami, et al., Life-long suppression of growth hormone-insulin-like growth factor I activity in genetically altered rats could prevent age-related renal damage, Endocrinology 147 (2006) 5690–5698.
[25] R.N. Fine, Growth hormone and the kidney: the use of recombinant human growth hormone (rhGH) in growth-related children with chronic renal insufficiency, J. Am. Soc. Nephrol. 1 (1991) 1139–1145.
[26] A.M. el Nahas, The role of growth hormone and insulin-like growth factor-1 in experimental renal growth and scarring, Am. J. Kidney Dis. 17 (1991) 677–679.
[27] C.J. Quaife, L.S. Mathews, C.A. Pinkert, et al., Histopathology associated with elevated levels of growth hormone and insulin-like growth factor I in transgenic mice, Endocrinology 124 (1989) 40–48.
[28] B. Feldt-Rasmussen, M. El Nahas, Potential role of growth factors with particular focus on growth hormone and insulin-like growth factor-1 in the management of chronic kidney disease, Semin. Nephrol. 29 (2009) 50–58.
[29] C. He, C. Esposito, C. Phillips, et al., Dissociation of glomerular hypertrophy, cell proliferation, and glomerulosclerosis in mouse strains heterozygous for a mutation (Os) which induces a 50% reduction in nephron number, J. Clin. Invest. 97 (1996) 1242–1249.
[30] M.M. Rechler, Insulin-like growth factor binding proteins, Vitam. Horm. 47 (1993) 1–114.
[31] P.D. Lee, L.C. Giudice, C.A. Conover, et al., Insulin-like growth factor binding protein-1: recent findings and new directions, Proc. Soc. Exp. Biol. Med. 216 (1997) 319–357.
[32] B. Tonshoff, D. Kiepe, S. Ciarmatori, Growth hormone/insulin-like growth factor system in children with chronic renal failure, Pediatr. Nephrol 20 (2005) 279–289.
[33] R. Hirschberg, S. Adler, Insulin-like growth factor system and kidney: physiology pathophysiology, and therapeutic implication, Am. J. Kidney Dis. 31 (1998) 901–919.
[34] E. Chin, C. Bondy, Insulin-like growth factor system gene expression in the human kidney, J. Clin. Endocrinol. Metab. 75 (1992) 962–968.

Hepatology Research

Hepatology Research 2010; 40: 438–445 doi: 10.1111/j.1872-034X.2009.00615.x

Short Communication

Identification of a novel biomarker for oxidative stress induced by hydrogen peroxide in primary human hepatocytes using the 2-nitrobenzenesulfenyl chloride isotope labeling method

Yoichiro Takami,[1,2] Hirofumi Uto,[1] Tsutomu Tamai,[1] Yuko Sato,[2] Yo-ichi Ishida,[2] Hiroyuki Morinaga,[3] Yoichi Sakakibara,[2,4] Akihiro Moriuchi,[1] Makoto Oketani,[1] Akio Ido,[1] Tomoaki Nakajima,[5] Takeshi Okanoue[6] and Hirohito Tsubouchi[1]

[1]Department of Digestive and Lifestyle-related Disease, Health Research, Human and Environmental Sciences, Kagoshima University Graduate School of Medical and Dental Sciences, Kagoshima, [2]Miyazaki Prefectural Industrial Support Foundation, [3]Research Institute, Unkai Shuzo, [4]Department of Biochemistry and Applied Biosciences, Faculty of Agriculture, University of Miyazaki, Miyazaki, [5]Molecular Gastroenterology and Hepatology, Graduate School of Medical Science, Kyoto Prefectural University of Medicine, Kyoto and, [6]Department of Hepatology, Saiseikai Suita Hospital, Osaka, Japan

Aim: Oxidative stress is involved in the progression of non-alcoholic steatohepatitis (NASH). However, there are few biomarkers that are easily measured and accurately reflect the disease states. The aim of this study was to identify novel oxidative stress markers using the 2-nitrobenzenesulfenyl (NBS) stable isotope labeling method and to examine the clinical utility of these diagnostic markers for NASH.

Methods: Proteins extracted from phosphate buffered saline- and hydrogen peroxide-loaded human primary hepatocyte were labeled with the [^{12}C]- and [^{13}C]-NBS reagents, respectively. Pairs of peaks with 6-Da differences in which the [^{13}C]-NBS labeling was more intense than the [^{12}C]-NBS labeling were detected by MALDI-TOF/MS and identified by MS/MS ion searching.

Results: Four pairs of peaks, m/z 1705–1711, m/z 1783–1789, m/z 1902–1908 and m/z 2790–2796, were identified as cytochrome c oxidase VIb (COX6B), liver carboxylesterase 1 (CES1), carbamoyl-phosphate synthase 1 (CPS1) and superoxide dismutase (MnSOD), respectively. Furthermore, serum MnSOD protein levels were significantly higher in NASH patients than in simple steatosis (SS) patients. The serum MnSOD levels tended to increase in parallel with the stage of fibrosis.

Conclusion: The NBS labeling technique was useful to identify biomarkers. Serum MnSOD may be a useful biomarker that can distinguish between SS and NASH.

Key words: 2-nitrobenzenesulfenyl, oxidative stress, MnSOD, non-alcoholic steatohepatitis

INTRODUCTION

IN SEVERAL LIVER diseases, including non-alcoholic steatohepatitis (NASH) and chronic hepatitis C (CHC), oxidative stress is a major pathogenetic event. Lipid peroxidation, free radical generation, CYP2E1 induction and mitochondrial dysfunction are known to induce oxidative stress and contribute to the progression of NASH and CHC.[1–3] Therefore, oxidative stress markers should be biomarkers that reflect the pattern and strength of oxidative stress and disease progression. Several oxidative stress markers for liver diseases including 8-hydroxy-2′-deoxyguanosine (8-OHdG), superoxide dismutase (SOD) and thioredoxin are well known. However, the clinical significance of these markers has not been fully evaluated.[4–6] Thus, oxidative stress markers that accurately reflect disease states and

Correspondence: Dr Hirofumi Uto; Department of Digestive and Lifestyle-related Disease, Health Research, Human and Environmental Sciences, Kagoshima University Graduate School of Medical and Dental Sciences, 8-35-1 Sakuragaoka, Kagoshima, 890-8520, Japan. Email: hirouto@m2.kufm.kagoshima-u.ac.jp
Received 11 May 2009; revision 14 September 2009; accepted 22 September 2009.

can be easily measured are necessary to accurately diagnose NASH or CHC.

In recent years, proteomic techniques, including 2-D gel electrophoresis (2-DE), have been commonly used to explore novel biomarkers. However, traditional 2-DE-based proteomic approaches are tedious and have several limitations, including reduced sensitivity and lack of quantitative results. Isotope-coded affinity tagging (ICAT) and isotope tagging for relative and absolute quantitation (iTRAQ) are the most commonly used chemical isotope labeling methods and can be used to address many of the limitations of 2-DE. In this report, we examined a novel stable isotope labeling method, the 2-nitrobenzenesulfenyl (NBS) labeling method developed by Kuyama *et al.*[7] The NBS labeling method is based on the specific binding reaction of the NBS reagent to tryptophan residues within a protein, and the 6-Da mass difference between [^{12}C]-NBS-labeled and [^{13}C]-NBS-labeled peptides generates a mass signature for all tryptophan-containing peptides.[7,8]

Here, we explored novel oxidative stress marker candidates using the NBS labeling method and identified four candidate oxidative stress markers in human primary hepatocytes including MnSOD. Furthermore, we verified the clinical significance of MnSOD as a diagnostic marker for NASH.

METHODS

Chemicals and materials

THE ^{13}CNBS® STABLE isotope labeling kit-N was purchased from Shimadzu Biotech (Kyoto, Japan). Human primary hepatocytes (a monolayer of human long-term hepatocytes), which were isolated from a 77-year-old woman, were purchased from Biopredic International (Rennes, France). 4-Hydroxycinnamic acid (CHCA) was obtained from Bruker Daltonics (Bremen, Germany) and 3-hydroxy-4-nitrobenzoic acid (3H4NBA) was purchased from Sigma Chemical (St Louis, MO, USA). Sequencing-grade modified trypsin was from Promega (Madison, WI, USA), and the protease inhibitor cocktail set III was from Calbiochem (Darmstadt, Germany).

Cell culture, NBS labeling and identification of NBS-labeled peptides

Human primary hepatocytes were cultured in a long-term culture medium.[9] Confluent human primary hepatocytes (~2×10^6 cells/12.5 cm^2 flask) were incubated for 24 h with phosphate buffered saline (PBS) or 200 μM hydrogen peroxide (H_2O_2).[10,11] Cells were washed and homogenized in 50 mM phosphate buffer, pH 8.0, containing 1% protease inhibitor cocktail set III. The NBS labeling was performed as previously described.[12,13] Briefly, both cell lysates (100 μg) treated with PBS or H_2O_2 were labeled with [^{12}C]- or [^{13}C]-NBS under acidic conditions, respectively. After labeling, the two respective conditioned protein mixtures were denatured with urea and reduced with tris(2-carboxyethyl)phosphine (TCEP) followed by alkylation with iodoacetamide. NBS-labeled proteins were digested with trypsin and eluted through phenyl sepharose using a stepwise gradient of increasing acetonitrile (10%, 15%, 20%, 25%, 30%, 35%, 40%, 45% and 50%) containing 0.1% trifluoro acetate. Next, the NBS-labeled peptides were ionized by a combined application of CHCA and 3H4NBA as described.[14,15] The mass spectral data were obtained by MALDI-TOF-TOF-MS, Autoflex II TOF/TOF (Bruker Daltonics) in positive-ion and reflectron mode. Pairs of peaks with a 6-Da difference were identified by MS/MS ion searching using tandem MS. The data set from the MS/MS ion was analyzed using the database search engine, Mascot (www.matrixscience.com), to find the closest match with known proteins/peptides in the database from the Swiss-Prot website.

Western blot analysis

Equal amounts of cell lysates from human primary hepatocytes (4 μg) were run on sodium dodecylsulfate polyacrylamide gels and electroblotted onto polyvinylidene fluoride membranes. The blots were probed with anti-cytochrome *c* oxidase VIb isoform 1 (anti-COX6B), anti-liver carboxylesterase 1 (anti-CES1), anti-carbamoyl-phosphate synthase [ammonia] mitochondrial 1 (anti-CPS1) and anti-MnSOD antibodies. After incubating the membrane with the appropriate horseradish peroxidase-conjugated secondary antibody, the reactivity was visualized using an ECL chemiluminescent detection kit (GE Healthcare Biosciences, Tokyo, Japan).

Real-time reverse transcription polymerase chain reaction (RT–PCR)

Total RNA was extracted from cells using ISOGEN (Nippon Gene, Toyama, Japan) according to the manufacturer's instructions. Samples were reverse-transcribed using the PrimeScript RT reagent Kit (TAKARA Bio, Shiga, Japan). Synthesized cDNA was amplified using SYBR Premix Ex Taq II (TAKARA Bio) and analyzed by StepOnePlus Real-Time PCR Systems and StepOne

Table 1 Identification and quantification of 2-nitrobenzenesulfenyl-labeled peak pairs

Accession no.	Protein name	Peak pairs (^{12}C–^{13}C, m/z)	Identified sequences
P14853	Cytochrome *c* oxidase subunit VIb isoform 1	1705–1711	NC**W**QNYLDFHR
P23141	Liver carboxylesterase 1 precursor	1783–1789	FTPPQPAEP**W**SFVK
P31327	Carbamoyl-phosphate synthase [ammonia], mitochondrial precursor	1902–1908	GAEVHLVP**W**NHDFTK
P04179	Superoxide dismutase [Mn], mitochondrial precursor	2790–2796	FNGGGHINHSIF**W**TNLSPNGGGEPK

Bold and underlined characters highlight the tryptophan (W) residues in the identified peptide sequences.

Software ver. 2.0 (Applied Biosystems, Foster City, CA, USA). The cycle conditions were as follows: one cycle at 95°C for 30 s followed by 35 cycles each at 95°C for 5 s and 60°C for 34 s. To normalize the amount of total RNA present in each reaction, the glyceraldehydes 3-phosphate dehydrogenase (GAPDH) gene was used as an internal standard.

Serum samples and MnSOD enzyme-linked immunosorbent assay (ELISA)

Serum samples were obtained from 20 healthy subjects, 15 simple steatosis (SS) patients and 29 NASH patients after a thorough clinical evaluation. Signed informed consent was obtained from each patient. The patients were diagnosed at University Hospital, Kyoto Prefectural University of Medicine (Kyoto, Japan) and Kagoshima University (Kagoshima, Japan). The study protocol was approved by the Ethics Committee of the Kagoshima University Hospital, the Kyoto Prefectural University of Medicine and the Miyazaki Prefectural Industrial Support Foundation. Serum MnSOD levels were measured by a Human Superoxide Dismutase 2 ELISA (AbFRONTIER, Seoul, Korea).

Statistical analysis

Differences among three groups were evaluated using Kruskal–Wallis test followed by Dunn's multiple comparison test. Correlation coefficients were calculated by Spearman's rank correlation analysis. A receiver-operator curve (ROC) was constructed by plotting the sensitivity and specificity (100 – specificity) for each value.

RESULTS

THE NBS-LABELED peptides from human primary hepatocytes were analyzed by MALDI-TOF/MS, and 73 pairs of peaks with 6-Da differences were detected in all mass spectra. Among these pairs of peaks, 44 pairs had a greater signal intensity in the H_2O_2-loaded sample compared to the PBS-loaded sample (data not shown). Among these 44 pairs of peaks, four peak pairs, m/z 1705–1711, m/z 1783–1789, m/z 1902–1908 and m/z 2790–2796, were identified as COX6B, CES1, CPS1 and superoxide dismutase (Mn), mitochondrial (MnSOD), respectively, by MS/MS ion searching (Table 1). The MS spectrum of the m/z 2790–2796 pair and the MS/MS spectrum of 2796 m/z ([^{13}C]-NBS labeled; MnSOD) are shown in Figure 1(a,b), respectively. Western blotting and real-time RT–PCR revealed that the protein and mRNA expression for each of these molecules increased in human primary hepatocytes after H_2O_2 loading (Fig. 1c–e).

Figure 1 Typical MS spectrum and MS/MS spectra from a proteomic analysis. (a) MALDI-TOF/MS spectra of a pair of peaks, 2790–2796 m/z, and the relative intensities of the [^{13}C]-2-nitrobenzenesulfenyl (NBS)-labeled peak compared to the [^{12}C]-NBS-labeled peak. Relative intensities are the means of two independent values analyzed by Autoflex II TOF/TOF. (b) MS/MS spectra of 2796 m/z ([13C]-NBS-labeled). From the detected MS/MS spectra, superoxide dismutase (Mn) mitochondrial was identified. (c) Equal amounts of cell extracts (4 μg) from human primary hepatocytes loaded with 200 μM hydrogen peroxide (H_2O_2) for 24 h were separated by sodium dodecylsulfate polyacrylamide gel electrophoresis and then immunoblotted with cytochrome *c* oxidase VIb isoform 1 (COX6B)-, liver carboxylesterase 1 (CES1)-, carbamoyl-phosphate synthase (ammonia), mitochondrial 1 (CPS1)-, superoxide dismutase [Mn], mitochondrial (MnSOD)- or β-actin-specific antibodies. (d) Quantitative representation of the western blot data. The results have been normalized to β-actin levels and are expressed as the levels relative to untreated cells. The data are the means of duplicate cultures. (e) The mRNA expression levels of COX6B, CES1, CPS1, MnSOD and glyceraldehyde 3-phosphate dehydrogenase (GAPDH) were measured by real-time polymerase chain reaction. The results have been normalized to GAPDH and are expressed as the levels relative to untreated cells. The data are the means of duplicate cultures. PBS, phosphate buffered saline.

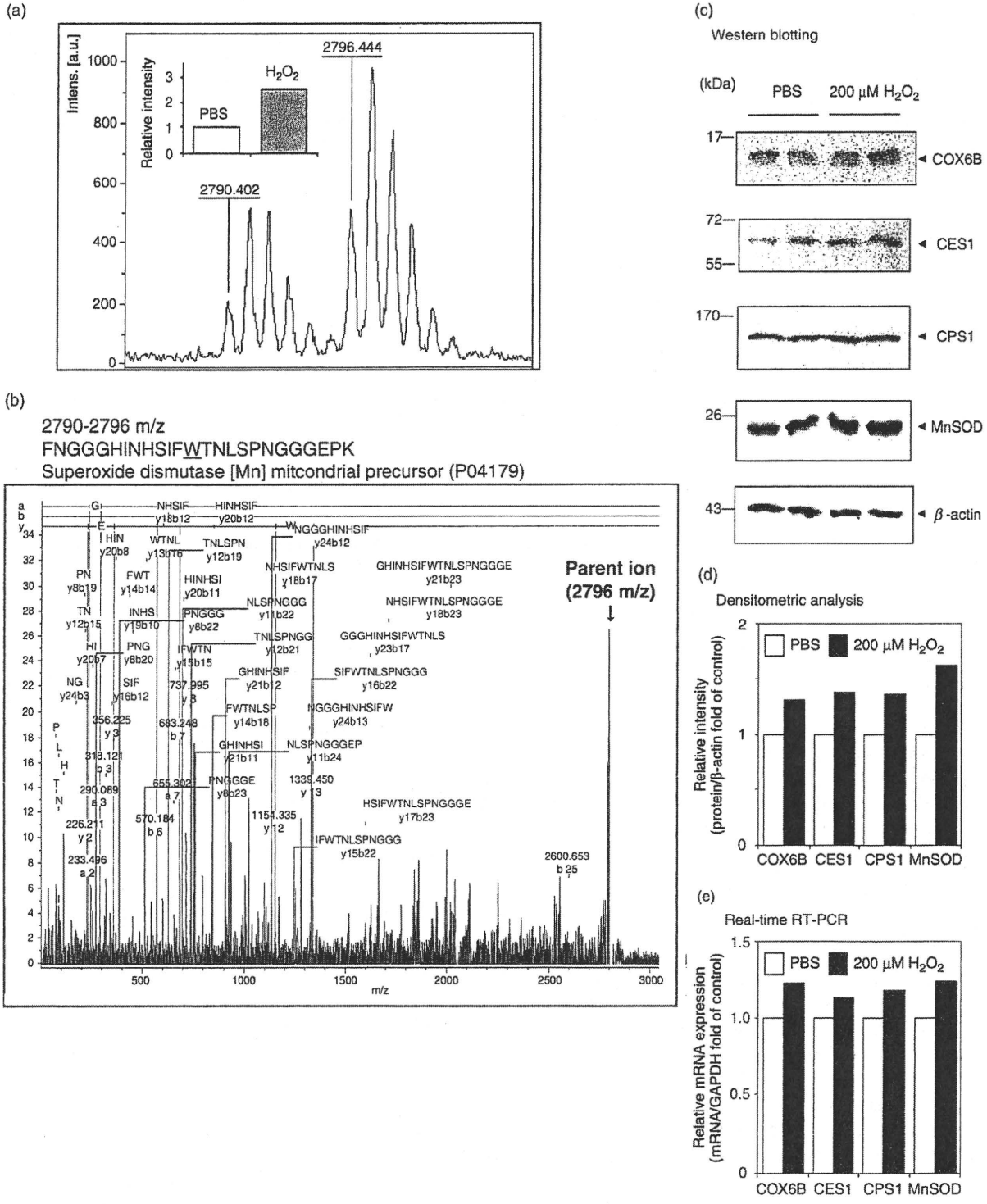

Table 2 Characteristics of study subjects

	Simple steatosis ($n = 15$)	NASH ($n = 29$)	*P*-value
Age (years)	43.2 ± 14.0	60.8 ± 14.9	**<0.001**
Sex (male/female)	11/4	11/18	**<0.05**
Height (cm)	162.5 ± 11.2	156.5 ± 8.7 (28)	0.05
Bodyweight (kg)	69.3 ± 11.8	69.2 ± 15.2 (28)	0.58
BMI (kg/m^2)	26.3 ± 3.6	28.1 ± 4.4 (28)	0.23
Diabetes (yes/no)	5/10	13/15 (28)	0.52
Hyperlipidemia (yes/no)	10/5	16/12 (28)	0.74
Hypertension (yes/no)	4/11	10/18 (28)	0.74
Hb (g/dL)	15.1 ± 1.8	14.4 ± 1.5	0.07
Plt (×10^4/μL)	23.8 ± 7.5	18.8 ± 7.0	**<0.05**
AST (IU/L)	41.6 ± 20.2	69.4 ± 46.5	**<0.05**
ALT (IU/L)	83.1 ± 53.1	94.6 ± 96.0	0.89
γ-GTP (U/L)	75.3 ± 52.4	155.6 ± 303.1	0.40
ChE (IU/L)	417.9 ± 97.5	352.8 ± 135.5	**<0.05**
γ-Glob (g/dL)	1.27 ± 0.40	1.50 ± 0.44 (24)	0.06
Total cholesterol (mg/dL)	209.2 ± 45.8	204.8 ± 52.1	0.97
Triglyceride (mg/dL)	168.3 ± 65.8	184.8 ± 168.3	0.45
BS (mg/dL)	119.1 ± 48.5	112.3 ± 34.3	0.61
Ferritin (mg/dL)	190.0 ± 112.7 (14)	239.8 ± 234.3 (22)	0.75

Values represent means ± standard deviation for the indicated number of subjects. Significant differences between the mean values ($P < 0.05$) were assessed by Fisher's exact probability test (sex, diabetes, hyperlipidemia and hypertension) or Mann–Whitney's *U*-test (other items).
Values in parentheses indicate the number of samples. Bold characters highlight statistically significant *P*-values.
ALT, alanine aminotransferase; AST, aspartate aminotransferase; BMI, body mass index; BS, blood sugar; ChE, choline esterase; γ-Glob, γ-globulin; γ-GTP, γ-glutamyl transpeptidase; Hb, hemoglobin; NASH, non-alcoholic steatohepatitis; Plt, platelet count.

The clinical characteristics of the SS and NASH groups were not significantly different except for the average age, platelet count (Plt), aspartate aminotransferase (AST) and choline esterase (ChE) (Table 2). We examined the serum MnSOD levels in healthy subjects ($n = 20$), SS patients ($n = 15$) and NASH patients ($n = 29$). There were no significant differences in MnSOD serum levels between healthy subjects and SS patients (Fig. 2a). In contrast, NASH patients had significantly higher serum MnSOD levels than both healthy subjects and SS patients (Fig. 2a). In addition, as shown in Figure 2(b), the serum levels of MnSOD tended to increase in parallel with the fibrosis stage. In contrast, there was no correlation between the levels of MnSOD and the activity grade of NASH (Fig. 2c). ROC of MnSOD levels were constructed to distinguish NASH (29 patients) from SS (15 patients) (Fig. 2d). The serum MnSOD threshold level that was used to predict NASH was calculated to be 71.8 ng/mL. At this threshold, the sensitivity was 69.0% and the specificity was 80.0%. The area under the ROC (AUC) for serum MnSOD levels was 0.760 ($P = 0.010$). The ROC curves for Plt, AST and ChE, which were significantly different between SS and NASH (Table 2), were also constructed. As a result, the AUC (*P*-value, threshold, sensitivity [%], specificity [%]) for Plt, serum AST and ChE were 0.733 (0.012, 19.4, 65.5, 86.7), 0.726 (0.015, 42.0, 65.5, 73.3) and 0.687 (0.044, 317.5, 48.3, 86.7), respectively.

DISCUSSION

IN THIS REPORT, we used the NBS labeling method to identify novel oxidative stress markers in hepatocytes that can be used as diagnostic markers for NASH and identified four candidate markers, COX6B, CES1, CPS1 and MnSOD, that were upregulated with H_2O_2 loading (Table 1, Fig. 1). Several recent studies have reported novel approaches that combine the NBS labeling method with 2-DE, high-performance liquid chromatography (HPLC) and lectin column chromatographic techniques.[13–16] In our present study, we identified only four proteins, indicating that it may be necessary to modify the current method by 2-DE and column chromatographic techniques to identify additional NBS-

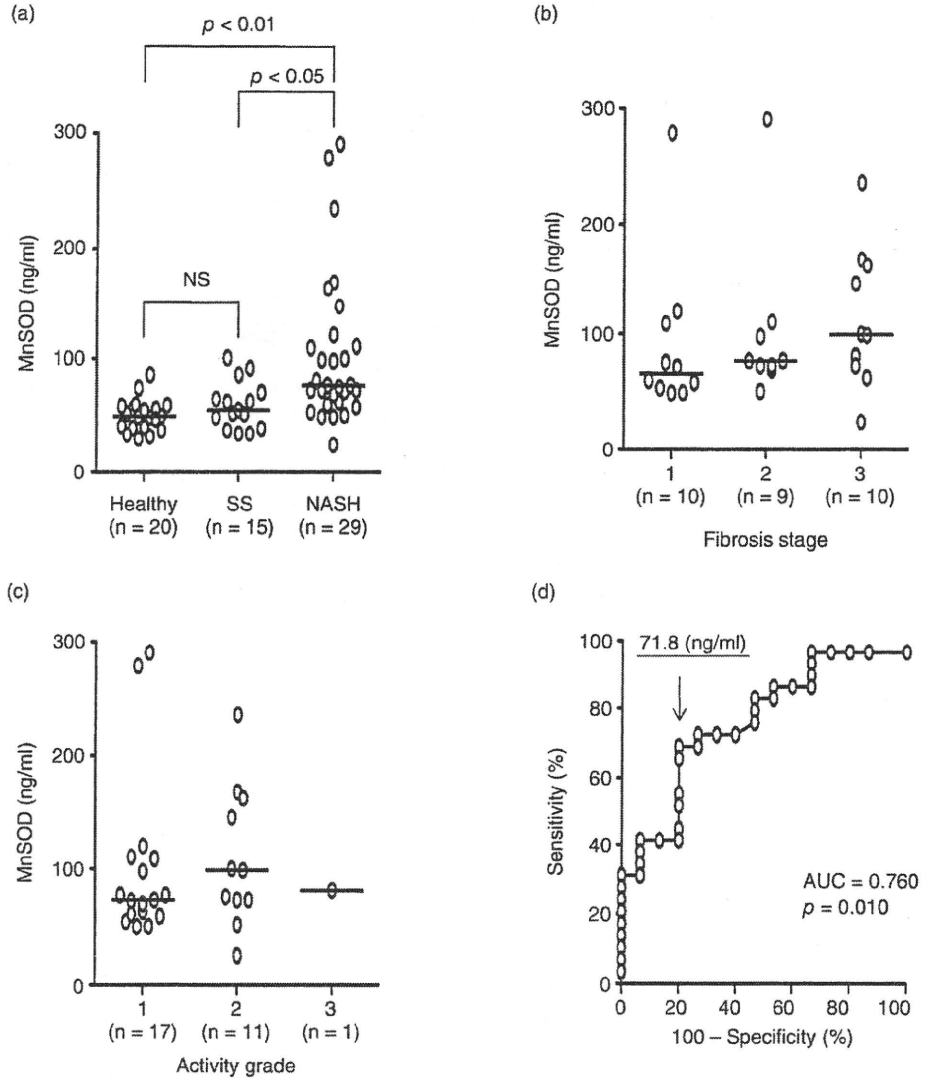

Figure 2 Clinical significance of serum MnSOD levels. (a) Serum MnSOD levels in healthy subjects and patients with SS or non-alcoholic steatohepatitis (NASH). Serum MnSOD levels were measured by enzyme-linked immunosorbent assay. (b) Comparison between serum MnSOD levels and the fibrosis stage in SS and NASH patients. (c) Comparison between serum MnSOD levels and the activity grade in SS and NASH patients. (d) Receiver–operator curve for MnSOD. The differences among three groups were evaluated using Kruskal–Wallis test followed by Dunn's multiple comparison test. Correlation coefficients were calculated by Spearman's rank correlation analysis. Bars indicate the median in the respective groups. AUC, area under the curve.

labeled peptides. In addition, further studies are needed to identify novel biomarkers by other proteomic techniques using serum samples from SS and NASH patients.

COX6B, CPS1 and MnSOD are mitochondrial proteins, and therefore may be indicators of mitochondrial disorders that are induced by oxidative stress. CPS1 is expressed primarily in the liver and small intestine and is involved in the urea cycle.[17] In galactosamine-induced rat acute hepatitis, plasma concentrations of CPS1 increase up to approximately 100-fold for 24 h after treatment.[18] This may indicate that secreted CPS1 is a serum marker for acute hepatitis. CES1, which is responsible for detoxification of exogenous compounds such

as esters, amides and thioesters, is also known to exist in the serum. Therefore, CES1, like CPS1, may be a serum oxidative stress marker.[19,20] Additional studies are needed to further evaluate the serum levels of these identified proteins.

MnSOD primarily exists in the mitochondrial matrix and eliminates reactive oxygen species (ROS) by catalyzing the dismutation of superoxide radicals and hydrogen peroxide.[19] Furthermore, MnSOD expression was previously shown to increase after exposure to hydrogen peroxide in rat hepatocytes.[21] In addition, obese mice were previously reported to have increased hepatic H_2O_2 levels and necrosis following an imbalance between increased MnSOD, which forms H_2O_2, and decreased glutathione activity, which detoxifies H_2O_2.[22] We found that MnSOD is potentially a novel diagnostic marker of NASH that can be used to distinguish between SS and NASH. One of the mechanisms contributing to increased MnSOD serum levels in NASH might be the discharge of MnSOD from necrotic hepatocytes. On the other hand, in the liver, several pro-inflammatory cytokines, such as tumor necrosis factor-α, interleukin-6 and interleukin-1β can act as common inducers of NASH.[23,24] Such pro-inflammatory cytokines have been shown to induce MnSOD expression in liver tissues.[25] Furthermore, pro-inflammatory cytokines induced the expression and secretion of MnSOD in several cancer cell lines including hepatoma cells.[26,27] In our present study, the origin of MnSOD produced in NASH and the precise mechanism of increased serum levels of MnSOD in NASH patients remain unclear. However, these reports may partially support the mechanism of MnSOD production in NASH. Further elucidation is necessary to clarify the mechanism of MnSOD expression and production in NASH.

Several reports have shown a relationship between the enzymatic activity of MnSOD and non-alcoholic fatty liver disease, NASH, liver cirrhosis and hepatocellular carcinoma.[28-31] Ono *et al.* showed that MnSOD serum levels were significantly increased in patients with primary biliary cirrhosis compared to patients with other liver diseases.[32] However, the serum protein levels of MnSOD in liver diseases have not been fully evaluated. In addition, the enzymatic activity of serum MnSOD was not different among the three groups and this activity did not correlate with serum MnSOD levels in our study (data not shown). The reasons for these results are unclear. However, as shown in Figure 2(b), serum MnSOD levels increased in parallel with the stage of fibrosis in NASH. The increase in serum MnSOD levels also significantly correlated with the serum AST levels (data not shown). These results indicate that serum MnSOD might be a biomarker that reflects hepatitic and fibrotic pathology. In addition, although MnSOD levels should increase in patients with other diseases including CHC, ROC analysis revealed that serum MnSOD may be a more sensitive biomarker than Plt, AST and ChE. We concluded that serum MnSOD is a useful biomarker that can distinguish SS and NASH.

ACKNOWLEDGMENTS

THIS WORK WAS supported in part by Grants-in-Aid for Scientific Research (C) from the Japan Society for the Promotion of Science (JSPS), Research for Promoting Technological Seeds (A) from the Japan Science and Technology Agency (JST), the Collaboration of Regional Entities for the Advancement of Technological Excellence (CREATE) from the JST, and a Grant-in-Aid (Research on Hepatitis and BSE) from the Ministry of Health, Labor and Welfare of Japan.

REFERENCES

1 Leclercq IA, Farrell GC, Field J, Bell DR, Gonzalez FJ, Robertson GR. CYP2E1 and CYP4A as microsomal catalysts of lipid peroxides in murine nonalcoholic steatohepatitis. *J Clin Invest* 2000; **105**: 1067–75.
2 Piccoli C, Scrima R, D'Aprile A *et al.* Mitochondrial dysfunction in hepatitis C virus infection. *Biochim Biophys Acta* 2006; **1757**: 1429–37.
3 Perez-Carreras M, Del Hoyo P, Martin MA *et al.* Defective hepatic mitochondrial respiratory chain in patients with nonalcoholic steatohepatitis. *Hepatology* 2003; **38**: 999–1007.
4 Wu LL, Chiou CC, Chang PY, Wu JT. Urinary 8-OHdG: a marker of oxidative stress to DNA and a risk factor for cancer, atherosclerosis and diabetics. *Clin Chim Acta* 2004; **339**: 1–9.
5 Fujii J, Taniguchi N. Phorbol ester induces manganese-superoxide dismutase in tumor necrsis factor-resistant cells. *J Biol Chem* 1991; **266**: 23142–6.
6 Nishinaka Y, Masutani H, Nakamura H, Yodoi J. Regulatory roles of thioredoxin in oxidative stress-induced cellular responses. *Redox Rep* 2001; **6**: 289–95.
7 Kuyama H, Watanabe M, Toda C, Ando E, Tanaka K, Nishimura O. An approach to quantitative proteome analysis by labeling tryptophan residues. *Rapid Commun Mass Spectrom* 2003; **17**: 1642–50.
8 Matsuo E, Toda C, Watanabe M *et al.* Improved 2-nitrobenzenesulfenyl method: optimization of the protocol and improved enrichment for labeled peptides. *Rapid Commun Mass Spectrom* 2006; **20**: 31–8.

9 Lanford RE, Carey KD, Estlack LE, Smith GC, Hay RV. Analysis of plasma protein and lipoprotein synthesis in long-term primary cultures of baboon hepatocytes maintained in serum-free medium. *In Vitro Cell Dev Biol* 1989; **25**: 174–82.
10 Rosseland CM, Wierod L, Oksvold MP *et al.* Cytoplasmic retention of peroxide-activated ERK provides survival in primary cultures of rat hepatocytes. *Hepatology* 2005; **42**: 200–7.
11 Conde de la Rosa L, Schoemaker MH, Vrenken TE *et al.* Superoxide anions and hydrogen peroxide induce hepatocyte death by different mechanisms: involvement of JNK and ERK MAP kinases. *J Hepatol* 2006; **44**: 918–29.
12 Matsuo E, Toda C, Watanabe M *et al.* Selective detection of 2-nitrobenzenesulfenyl-labeled peptides by matrix-assisted laser desorption/ionization-time of flight mass spectrometry using a novel matrix. *Proteomics* 2006; **6**: 2042–9.
13 Sumida Y, Nakashima T, Yoh T *et al.* Serum thioredoxin levels as a predictor of steatohepatitis in patients with non-alcoholic fatty liver disease. *J Hepatol* 2003; **38**: 32–8.
14 Ou K, Kesuma D, Ganesan K *et al.* Quantitative profiling of drug-associated proteomic alterations by combined 2-nitrobenzenesulfenyl chloride (NBS) isotope labeling and 2DE/MS identification. *J Proteome Res* 2006; **5**: 2194–206.
15 Iida T, Kuyama H, Watanabe M *et al.* Rapid and efficient MALDI-TOF MS peak detection of 2-nitrobenzenesulfenyl-labeled peptides using the combination of HPLC and an automatic spotting apparatus. *J Biomol Tech* 2006; **17**: 333–41.
16 Ueda K, Katagiri T, Shimada T *et al.* Comparative profiling of serum glycoproteome by sequential purification of glycoproteins and 2-nitrobenzensulfenyl (NBS) stable isotope labeling: a new approach for the novel biomarker discovery for cancer. *J Proteome Res* 2007; **6**: 3475–83.
17 Pearson DL, Dawling S, Walsh WF *et al.* Neonatal pulmonary hypertension–urea-cycle intermediates, nitric oxide production, and carbamoyl-phosphate synthetase function. *N Engl J Med* 2001; **344**: 1832–8.
18 Ozaki M, Terada K, Kanazawa M, Fujiyama S, Tomita K, Mori M. Enzyme-linked immunosorbent assay of carbamoylphosphate synthethase 1: plasma enzyme in rat experimental hepatitis and its clearance. *Enzyme Protein* 1994–1995; **48**: 213–21.
19 Munger JS, Shi GP, Mark EA, Chin DT, Gerard C, Chapman HA. A serine esterase released by human alveolar macrophages is closely related to liver microsomal carboxylesterases. *J Biol Chem* 1991; **266**: 18832–8.
20 Yan B, Yang D, Bullock P, Parkinson A. Rat serum carboxylesterase. Cloning, expression, regulation, and evidence of secretion from liver. *J Biol Chem* 1995; **270**: 19128–34.
21 Kurobe N, Inagaki T, Kato K. Sensitive enzyme immunoassay for Mn superoxide dismutase. *Clin Chim Acta* 1990; **192**: 171–9.
22 Rohrdanz E, Kahl R. Alterations of antioxidant enzyme expression in response to hydrogen peroxide. *Free Radic Biol Med* 1998; **24**: 27–38.
23 Robin MA, Demeilliers C, Sutton A *et al.* Alcohol increases tumor necrosis factor a and decreases nuclear factor kB to activate hepatic apoptosis in genetically obese mice. *Hepatology* 2005; **42**: 1280–90.
24 Hotamisligil GS. Inflammation and metabolic disorders. *Nature* 2006; **444**: 860–7.
25 Shoelson SE, Lee J, Goldfine AB. Inflammation and insulin resistance. *J Clin Invest* 2006; **116**: 1793–801.
26 Sato M, Sasaki M, Hojo H. Antioxidative roles of metallothionein and manganese superoxide dismutase induced by tumor necrosis factor-α and interleukin-6. *Arch Biochem Biophys* 1995; **316**: 738–44.
27 Ono M, Kohda H, Kawaguchi T *et al.* Induction of Mn-superoxide dismutase by tumor necrosis factor, interleukin-1 and interleukin-6 in human hepatoma cells. *Biochem Biophys Res Commun* 1992; **182**: 1100–7.
28 Nakata T, Suzuki K, Fujii J, Ishikawa M, Taniguchi N. Induction and release of manganese superoxide dismutase from mitochondria of human umbilical vein endothelial cells by tumor necrosis factor-α and interleukin-1β. *Int J Cancer* 1993; **55**: 646–50.
29 Videla LA, Rodrigo R, Orellana M *et al.* Oxidative stress-related parameters in the liver of non-alcoholic fatty liver disease patients. *Clin Sci* 2004; **106**: 261–8.
30 Clemente C, Elba S, Buongiorno G *et al.* Manganese superoxide dismutase activity and incidence of hepatocellular carcinoma in patients with Child–Pugh class A liver cirrhosis: 7-year follow-up study. *Liver Int* 2007; **27**: 791–7.
31 Perlemuter G, Davit-Spraul A, Cosson C *et al.* Increase in liver antioxidant enzyme activities in non-alcoholic fatty liver disease. *Liver Int* 2005; **25**: 946–53.
32 Ono M, Sekiya C, Ohhira M *et al.* Elevated level of serum Mn-superoxide dismutase in patients with primary biliary cirrhosis: possible involvement of free radicals in the pathogenesis in primary biliary cirrhosis. *J Lab Clin Med* 1991; **118**: 476–83.

Hepatology Research

Hepatology Research 2010; 40: 337–345 doi: 10.1111/j.1872-034X.2009.00589.x

Original Article

Proanthocyanidin derived from the leaves of *Vaccinium virgatum* suppresses platelet-derived growth factor-induced proliferation of the human hepatic stellate cell line LI90

Yoichiro Takami,[1,2] Hirofumi Uto,[2] Masahiko Takeshita,[3] Hisahiro Kai,[1,4] Ena Akamatsu,[1] Akihiro Moriuchi,[2] Susumu Hasegawa,[2] Makoto Oketani,[2] Akio Ido,[2] Hiroaki Kataoka[5] and Hirohito Tsubouchi[2]

[1]Miyazaki Prefectural Industrial Support Foundation, [3]Research Division, Minami Nippon Dairy, [4]Faculty of Hygienic Chemistry, School of Pharmaceutical Sciences, Kyushu University of Health and Welfare, [5]Section of Oncopathology and Regenerative Biology, Faculty of Medicine, University of Miyazaki, Miyazaki, and [2]Digestive Disease and Lifestyle-Related Disease Health Research, Human and Environmental Sciences, Kagoshima University Graduate School of Medicine and Dental Sciences, Kagoshima, Japan

Aim: Hepatic stellate cell (HSC) proliferation plays a pivotal role in liver fibrogenesis, and agents that suppress HSC activation, including platelet-derived growth factor (PDGF)-induced HSC proliferation, are good candidates for antifibrogenic therapies. In this report, we use the LI90 HSC line to elucidate the antifibrogenic effects of proanthocyanidin derived from the leaves of *Vaccinium virgatum*.

Methods: Proanthocyanidin (PAC) was extracted from the leaves of blueberry *V. virgatum* (BB-PAC), grape seeds (GS-PAC) and *Croton lechleri* (CL-PAC). These extracts were examined for their effects on PDGF-BB-induced LI90 cell proliferation and DNA synthesis. Extracellular signal-regulated kinase (ERK) and Akt phosphorylation and PDGF receptor-β (PDGFR-β) expression were evaluated by western blot analysis.

Results: BB-PAC potently suppressed PDGF-BB-induced proliferation and DNA synthesis of LI90 cells. BB-PAC also suppressed PDGF-BB-induced DNA synthesis in primary cultured rat HSC. Moreover, GS-PAC and CL-PAC suppressed PDGF-BB-induced DNA synthesis in LI90 cells. In contrast, the monomeric PAC catechin and epicatechin and dimeric PAC procyanidin B2 only slightly suppressed PDGF-BB-induced DNA synthesis. Western blot analysis showed that BB-PAC completely or partially inhibited PDGF-BB-induced ERK and Akt phosphorylation, respectively. In addition, BB-PAC partially inhibited the PDGF-BB-induced degradation of PDGFR-β.

Conclusion: Our results suggest that BB-PAC suppresses activated HSC by inhibiting the PDGF signaling pathway. In addition, these results provide novel findings that may facilitate the development of antifibrogenic agents.

Key words: Akt, extracellular signal-regulated kinase, hepatic stellate cell, platelet-derived growth factor-β, platelet-derived growth factor, proanthocyanidin.

INTRODUCTION

HEPATIC STELLATE CELLS (HSC) play a pivotal role during liver fibrogenesis. After hepatic damage from viral infection, cholestasis, metabolic diseases, persistent alcohol abuse or autoimmune liver diseases and others, HSC proliferate and transform from quiescent HSC into activated myofibroblasts. These cells produce excessive amounts of extracellular matrix compounds and matrix degradation inhibitors, which can result in hepatic fibrosis and ultimately cirrhosis, the end stage of fibrosis.[1,2] The functions of HSC are modulated by several cytokines and growth factors including platelet-derived growth factor (PDGF), which is a potent mitogen for HSC that is primarily produced by specialized liver macrophages known as Kupffer cells.[3]

Correspondence: Dr Hirofumi Uto, Digestive Disease and Lifestyle-Related Disease Health Research, Human and Environmental Sciences, Kagoshima University Graduate School of Medicine and Dental Sciences, 8-35-1 Sakuragaoka, Kagoshima 890-8520, Japan. Email: hirouto@m2.kufm.kagoshima-u.ac.jp
Received 11 February 2009; revision 30 June 2009; accepted 24 July 2009.

PDGF-induced HSC proliferation plays a critical role in hepatic fibrogenesis. Therefore, agents that suppress PDGF-induced HSC proliferation are potential candidates for antifibrogenic therapies.

Recent research has focused on identifying naturally occurring antifibrotic compounds that target PDGF-induced HSC proliferation or the production of collagen, transforming growth factor (TGF)-β and matrix metalloproteinases. A diverse range of natural products obtained from foods, including polyphenols, alkaloids and terpenoids, have been suggested to have an inhibitory effect on HSC,[4–9] and these products may provide novel therapeutic agents for hepatic fibrosis without side-effects. Proanthocyanidins (PAC) are naturally occurring polyphenols that are comprised of complicated mixtures, consisting primarily of polymers of flavan-3-ols such as catechin, epicatechin, gallocatechin, epigallocatechin, epigallocatechin-3-gallate (EGCG) and their dimeric and trimeric compounds. These PAC are derived from common foods such as tea, grapes, cranberries, almonds, chocolate and cacao beans.[10–14] Furthermore, it has been reported that drinking tea and coffee decreases the risk of clinically significant chronic liver disease.[15] In addition, EGCG, one of the green tea flavan-3-ols and a component of PAC, was previously shown to have a potent inhibitory effect on HSC proliferation.[3,16] However, the effect of other PAC components on HSC proliferation has not been fully elucidated.

The fruits and leaves of *Vaccinium virgatum* (blueberry), a member of the Ericaceae family, contain abundant levels of PAC that has a high ratio of polymerized PAC.[17,18] Therefore, patients with liver diseases such as hepatic fibrosis can easily consume these PAC by eating a diet rich in blueberries and other PAC-containing foods. However, it has not been reported whether the polymerized PAC found in natural foods such as blueberries also effectively prevent hepatic fibrosis and HSC proliferation.[19,20] Therefore, we extracted polymerized PAC from blueberry leaves (BB-PAC) and examined its effects on HSC proliferation and the DNA synthesis induced by PDGF-BB using the LI90 human HSC line and primary cultured rat HSC. Furthermore, we investigated the mechanism by which BB-PAC inhibits LI90 cell proliferation and DNA synthesis.

METHODS

PAC fractionation

A LYOPHILIZED POWDER of fresh *V. virgatum* Aiton leaves was kindly supplied by Unkai Shuzo (Miyazaki, Japan). The lyophilized powder (10 g) was sequentially extracted three times with *n*-hexane, ethyl acetate, and 100% methanol (100 mL, 30 min). The methanol extract was concentrated under reduced pressure to yield 3.5 g of extract. The extract (500 mg) was dissolved in 60% methanol, applied to a Sephadex LH-20 column, and successively separated with 60% methanol, 100% methanol and 70% acetone. The 70% acetone extract yielded approximately 100 mg of BB-PAC.[12] Grape seeds (Gravinol from Kikkoman, Chiba, Japan) and *Croton lechleri* (Sangre de Drago from Raintree Nutrition, Carson City, NV, USA) were extracted three times with 100% methanol (100 mL, 30 min), and then prepared as described above to yield GS-PAC and CL-PAC, respectively. Thiolysis was performed to characterize the polymerization states of these three PAC, including the mean degree of polymerization and the catechin composition.[21] EGCG and catechin were purchased from Kurita Analysis Service (Ibaragi, Japan). Epicatechin was purchased from Sigma (St Louis, MO, USA), and procyanidin B2 was purchased from Bio Chemika (Buchs, Switzerland).

Cell culture

The LI90 cell line was obtained from the Human Science Research Resources Bank (Osaka, Japan) and cultured in Dulbecco's minimal essential medium (DMEM; Sigma) supplemented with 10% fetal bovine serum (Medical & Biological Laboratories, Nagoya, Japan), 100 IU/mL penicillin and 50 mg/mL streptomycin. Cultures were incubated at 37°C in a humidified atmosphere with 5% CO_2, and the medium was changed weekly. We used LI90 cells with passage numbers between 20 and 26 for all experiments.

Isolation and culture of primary rat HSC

Hepatic stellate cells were isolated from male Sprague–Dawley rats (bodyweight, ~500 g) using collagenase and pronase as described previously.[22] HSC were identified by their typical star-like morphology under a light microscope, vitamin A-specific autofluorescence, and cellular expression of α-smooth muscle actin (α-SMA) detected using western blotting with α-SMA-specific antibodies. HSC were incubated in DMEM supplemented with 10% fetal bovine serum, 100 IU/mL penicillin and 50 mg/mL streptomycin. The medium was changed after 3 days and every 48 hours thereafter. Differentiated myofibroblasts generated after reseeding 14- to 18-day-old primary HSC were used in the experiments.

Measurement of cell proliferation, DNA synthesis and apoptosis

The 3-(4,5-dimethylthialzol-2-yl)-2,5-diphenyltetrazolium bromide (MTT) assay was performed as described previously.[23] Briefly, 5 mg/mL MTT was added to the culture in 1/10 the media volume. After a 2-h incubation, extraction buffer (12.8% sodium dodecylsulfate (SDS), 0.41 M acetate buffer at pH 4.5, and 32% *N,N*-dimethylformamide) was added, and the samples were incubated overnight at 37°C. The optical densities of the samples were measured at 570 nm using a plate reader. To evaluate DNA synthesis in LI90 cells, a 5-bromodeoxyuridine (BrdU)-specific enzyme-linked immunosorbent assay (ELISA) was performed using a 5-Bromo-2'-deoxy-uridine Labeling and Detection Kit III (Roche Diagnostics, Tokyo, Japan) according to the manufacturer's instructions. Briefly, LI90 cells that had been cultured under various conditions were incubated for 4–6 h with BrdU to allow incorporation into cellular DNA. Next, the cells were fixed in chilled 0.5 M ethanol/HCl fixative. Cellular BrdU incorporation was detected with peroxidase-conjugated anti-BrdU antibodies and quantified using a plate reader following the manufacturer's instructions. To evaluate DNA fragmentation in LI90 cells, DNA- and histone-specific ELISA were performed using Cell Death Detection ELISA^{PLUS} kits (Roche Diagnostics) according to the manufacturer's instructions. Briefly, cellular lysates were transferred into streptavidin-coated plates. Cellular histone and fragmented DNA were detected with biotin-conjugated anti-histone antibodies and peroxidase-conjugated anti-DNA antibodies, and quantified using a plate reader.

Western blot analysis

LI90 and primary rat HSC lysates were quantitatively examined using the Lowry method with bovine serum albumin as a standard. Equal amounts of cell lysates (5–10 μg) were separated on 8% or 10% SDS polyacrylamide gels (SDS-PAGE) and electroblotted onto polyvinylidine fluoride membranes. The blots were probed with antibodies specific for phospho-p44/42 mitogen-activated protein kinase (MAPK) (Thr202/Tyr204), phospho-stress-activated protein kinase/c-Jun N-terminal kinase (SAPK/JNK) (Thr183/Tyr185), p44/42 MAPK, phospho-Akt (Ser473), Akt, or PDGF receptor-β (Cell Signaling Technology, Danvers, MA, USA), α-SMA (DAKO, Carpinteria, CA, USA) or β-actin (Sigma). After incubating the membrane with horseradish peroxidase-conjugated secondary antibodies, reactivity was visualized using a Chemi Doc XRS-J digital densitometer (Bio-Rad Laboratories, Hercules, CA, USA) and electrogenerated chemiluminescence western blotting detection reagents (GE Healthcare Bio-sciences, Tokyo, Japan). Densitometric analysis was performed using Quantity One Software (Bio-Rad Laboratories).

Statistical analysis

All results are expressed as the means ± standard deviation (SD) of at least three independent experiments. A one-way ANOVA followed by Tukey's multiple comparison test was used to evaluate differences between groups.

RESULTS

PAC polymerization states

PROANTHOCYANIDINS FROM THREE different sources, BB-PAC, GS-PAC and CL-PAC, were prepared, and the polymerization states were analyzed by thiolysis. The results showed that the mean degree of polymerization for BB-PAC, GS-PAC and CL-PAC was 8.4, 14.4 and 8.3, respectively (data not shown). BB-PAC contained more epicatechin than GS-PAC and CL-PAC. On the other hand, GS-PAC and CL-PAC had higher levels of catechin than BB-PAC (data not shown). In addition, the BB-PAC sample contained approximately 10–30% dimeric and trimeric PAC, whereas these PAC forms were undetected in GS-PAC and CL-PAC (data not shown).

BB-PAC inhibits PDGF-BB-induced HSC proliferation

To determine the effect of BB-PAC on LI90 cell proliferation, LI90 cells were incubated for 96 h with 0.1–10 μg/mL BB-PAC, and viable cells were counted using the MTT method. BB-PAC decreased the viability of LI90 cells at concentrations greater than 3 μg/mL (Fig. 1a). LI90 cells were also incubated for 96 h with varying concentrations of BB-PAC, ranging 0.1–10 μg/mL, in the presence or absence of 10 ng/mL PDGF-BB. BB-PAC completely blocked PDGF-BB-induced cell proliferation at a concentration of 1 μg/mL (Fig. 1a). A BrdU-specific ELISA was used to determine whether 1 μg/mL BB-PAC inhibited the PDGF-BB-mediated enhancement in DNA synthesis. BB-PAC at 1 μg/mL completely inhibited PDGF-BB-induced DNA synthesis, whereas it did not affect DNA synthesis in the absence of PDGF-BB (Fig. 1b). In addition, 1 μg/mL BB-PAC significantly inhibited PDGF-BB-induced DNA synthesis in primary